

Submitted to *The Astronomical Journal*

The Centers of Early-Type Galaxies with *HST*. V. New WFPC2 Photometry ¹

Tod R. Lauer

National Optical Astronomy Observatory², P.O. Box 26732, Tucson, AZ 85726

S. M. Faber

UCO/Lick Observatory, Board of Studies in Astronomy and Astrophysics, University of California, Santa Cruz, CA 95064

Karl Gebhardt

Department of Astronomy, University of Texas, Austin, TX 78712

Douglas Richstone

Department of Astronomy, University of Michigan, Ann Arbor, MI 48109

Scott Tremaine

Princeton University Observatory, Peyton Hall, Princeton, NJ 08544

Edward A. Ajhar

Department of Natural Sciences, Mathematics, and Computer Sciences, St. Thomas University, Miami Gardens, FL 33054

M. C. Aller

Department of Astronomy, University of Michigan, Ann Arbor, MI 48109

Ralf Bender

Universitäts-Sternwarte, Scheinerstraße 1, München 81679, Germany

Alan Dressler

The Observatories of the Carnegie Institution of Washington, Pasadena, CA 91101

Alexei V. Filippenko

Department of Astronomy, University of California, Berkeley, CA 94720-3411

Richard Green

National Optical Astronomy Observatory, P.O. Box 26732, Tucson, AZ 85726

Carl J. Grillmair

SIRTF Science Center, Pasadena, CA 91125

Luis C. Ho

The Observatories of the Carnegie Institution of Washington, Pasadena, CA 91101

John Kormendy

Department of Astronomy, University of Texas, Austin, TX 78712

John Magorrian

Department of Physics, University of Durham, Durham, United Kingdom, DH1 3LE

Jason Pinkney

Department of Physics and Astronomy, Ohio Northern University, Ada, OH 45810

Christos Siopis

Department of Astronomy, University of Michigan, Ann Arbor, MI 48109

ABSTRACT

We present observations of 77 early-type galaxies imaged with the PC1 CCD of *HST*+WFPC2. “Nuker law” parametric fits to the surface brightness profiles are used to classify the central structure into “core” or “power-law” forms. Core galaxies are typically rounder than power-law galaxies. Nearly all power-laws with central ellipticity $\epsilon \geq 0.3$ have stellar disks, implying that disks are present in most power-laws with $\epsilon < 0.3$, but are not visible due to unfavorable geometry. A few low-luminosity flattened core galaxies also have disks; these may be transition forms from power-laws to more luminous core galaxies, which lack disks. Several core galaxies have strong isophote twists interior to their break radii, although power-laws have interior twists of similar physical significance when the photometric perturbations implied by the twists are evaluated. Central color gradients are typically consistent with the envelope gradients; core galaxies have somewhat weaker color gradients than power-laws. Nuclei are found in 29% of the cores and 60% of the power-laws. Nuclei are typically bluer than the surrounding galaxy. While some nuclei are associated with AGN, just as many are not; conversely, not all galaxies known to have low-level AGN exhibit detectable nuclei in the broad-band filters. NGC 4073 and 4382, are found to have central minima in their intrinsic starlight distributions; NGC 4382 resembles the double nucleus of M31. In general, the peak brightness location is coincident with the photocenter of the core

to a typical physical scale < 1 pc. Five galaxies, however, have centers significantly displaced from their surrounding cores; these may be unresolved asymmetric double nuclei. Lastly, as noted by previous authors, central dust is visible in about half of the galaxies. The presence and strength of dust correlates with nuclear emission, thus dust may outline gas that is falling into the central black hole. The prevalence of dust and its morphology suggest that dust clouds form, settle to the center, and disappear repeatedly on $\sim 10^8$ yr timescales. We discuss the hypothesis that cores are created by the decay of a massive black hole binary formed in a merger. Apart from their brightness profiles, there are no strong differences between cores and power-laws that demand this scenario; however, the rounder shapes of cores, their lack of disks, and their reduced color gradients may be consistent with it.

Subject headings: galaxies: nuclei — galaxies: photometry — galaxies: structure

1. Introduction

This paper presents *HST/WFPC2* observations of 77 early-type galaxies. We investigate the central morphology of the galaxies by characterizing the properties of their nuclei, color gradients, ellipticities, isophote twists, instances of central surface brightness minima, offset centers, dust content, and dust morphologies. The result is a more complete portrait of the sample galaxies than has been available heretofore and a reference where many different properties are measured and compared in one place. We also derive high resolution surface photometry profiles of the sample galaxies, which we characterize with “Nuker law” fits (Lauer et al. 1995). Analysis of the fit parameters is presented in Paper VI (Lauer et al., in preparation), in which we combine the present results with previously published Nuker law fits to *HST* surface photometry profiles to define an extended sample of 264 E/S0 galaxies.

A motivation of both this paper and Paper VI is to understand the origin of “cores” in early-type galaxies. *HST* images show that nearly all galaxies have singular starlight distributions in the sense that surface brightness diverges as $\Sigma(r) \sim r^{-\gamma}$, with $\gamma > 0$ (Lauer et al. 1991, 1992a,b; Crane et al. 1993; Kormendy et al. 1994; Ferrarese et al. 1994; Lauer et al. 1995). In typically lower-luminosity early-type galaxies, γ decreases only slowly as the center is approached and a steep $\gamma > 0.5$ cusp continues into the *HST* resolution limit; Lauer et al. (1995) classified these systems

¹Based on observations made with the NASA/ESA *Hubble Space Telescope*, obtained at the Space Telescope Science Institute, which is operated by the Association of Universities for Research in Astronomy, Inc., under NASA contract NAS 5-26555. These observations are associated with GO and GTO proposals # 5236, 5446, 5454, 5512, 5943, 5990, 5999, 6099, 6386, 6554, 6587, 6633, 7468, 7820, 8683, and 9107.

²The National Optical Astronomy Observatory is operated by AURA, Inc., under cooperative agreement with the National Science Foundation.

as “power-law” galaxies. In more luminous galaxies, however, the projected profile transitions or breaks from a steep power law in the envelope to a shallow inner cusp with $\gamma < 0.3$; these “core galaxies” thus show central deficits of starlight or a core compared to the centrally-steeper “power-law” galaxies. Many of the core galaxies are the same systems in which cores were already evident from ground-based observations (Kormendy 1985; Lauer 1985); however, rather than representing regions in which the central stellar density becomes constant, the residual shallow cusps in projected brightness still imply steep and singular cusps in density (Lauer et al. 1995).

Gebhardt et al. (1996) and Faber et al. (1997) showed that the distribution of cusp slopes at the *HST* resolution limit in both stellar luminosity density and projected surface brightness is bimodal; power-laws and core galaxies are separated into two distinct groups by their inner cusp slopes. Rest et al. (2001) and Ravindranath et al. (2001) later identified a small number of “intermediate” galaxies that have limiting cusp slopes with $0.3 < \gamma < 0.5$, but showed that the ensemble of cusp slopes in all early-type galaxies is still bimodal. This topic will be further explored in Paper VI, which strongly ratifies the bimodality of central structure.

Faber et al. (1997) also examined how the central structure correlates with other galaxy properties, showing that luminous early-type galaxies preferentially have cores, whereas most fainter spheroids have power-law profiles. Moreover, cores are slowly rotating and have boxy isophotes, while power laws rotate rapidly and are disk-like. These ideas resonate well with a revision of the Hubble sequence proposed by Kormendy & Bender (1996), which divided ellipticals into boxy, non-rotating types and disk-like, rotating types. The latter were seen to be the close relatives of spirals, whereas the boxy, non-rotating ellipticals were somehow “different.” Cores are associated with the boxy, non-rotating sequence, and thus serve as a fundamental morphological marker.

Faber et al. (1997) further argued that the prevalence of cores is directly tied to the presence of nuclear black holes in nearly all galaxies (Magorrian et al. 1998) and the assembly of galaxies by hierarchical mergers. Begelman et al. (1980) argued that the merging of two galaxies, each harboring a central massive black hole, would create a black hole binary in the center of the merger remnant. Gradual hardening of the binary via stellar encounters would scatter stars out of the center, creating a central deficit of stars with respect to inward extrapolation of the envelope in a merged galaxy whose center would otherwise be very dense. N-body simulations of merging galaxies with central black holes (Ebisuzaki et al. 1991; Makino 1997; Quinlan & Hernquist 1997; Milosavljević & Merritt 2001) show that cores can indeed form in such merger remnants. Looking for ways to test the hypothesis that cores reflect the effects of binary black holes on the central structure of galaxies is a subtext for much of the analysis presented in this paper. We will return to this topic in the summary.

A final section of the paper is devoted to the morphology and prevalence of optical dust absorption in early-type galaxies. As in previous works (e.g., de Koff et al. 2000, van Dokkum & Franx 1995, Tran et al. 2001), dust is found in roughly half of our galaxies. Dust is extremely well correlated with both the presence and strength of nuclear optical emission, which we assume

indicates AGN activity. Thus, it is hard to avoid concluding that dust is outlining interstellar material that is about to fall onto the black hole, and that it therefore becomes a valuable clue as to how that happens. We discuss the possibility that the diverse patterns of dust absorption seen in early-type galaxies may be viewed as various stages of a “settling sequence;” under this picture dust may come and go on timescales of a few $\times 10^8$ years. The implication is that galaxies might be emptying and refilling themselves with dust constantly, raising the question of where the dust comes from and why the process is cyclical. Understanding this could be an important clue to the growth of black holes.

2. Observations

2.1. The Sample

We present images and surface photometry for 77 early-type galaxies observed with *HST*+WFPC2; 55 of these were obtained under programs GO 5512, 6099, 6587, and 9107 which were carried out by our collaboration. The observations are listed in Table 1. We also include an independent reduction of the galaxies observed in GO 5454 (PI: Franx), which were selected to have kinematically decoupled cores (KDC). Analysis of these by Carollo et al. (1997) showed no morphological differences between ordinary ellipticals and those with KDC, thus including these galaxies in the present sample causes no obvious bias. Some of the remaining galaxies represent original or archival images obtained in support of GO 9107, in which we proposed STIS spectroscopy to explore the mass range of nuclear black holes at a particular galaxy luminosity. Lastly, there are additional galaxies obtained from the archive in support of our other STIS programs. A portion of this photometry has been published previously in papers on the detection of nuclear black holes (Kormendy et al. 1996; Gebhardt et al. 2000; Bower et al. 2001; Gebhardt et al. 2003) or on the morphology of galaxies with double centers or local minima in surface brightness at their centers (Lauer et al. 1996, 2002); such galaxies are presented again here to provide complete surface photometry in the context of a comprehensive re-investigation of the central structure of early-type galaxies. Table 1 lists any earlier publication of surface photometry derived from the given dataset.

There is no single criterion that characterizes our sample. In general, the sample comprises relatively luminous nearby elliptical and early-S0 galaxies that could be investigated spectroscopically with *HST* to detect and “weigh” nuclear black holes. The particular selection of galaxies was heavily informed by the central-structure parameter relationships presented by Faber et al. (1997). Several galaxies were selected, for example, within the luminosity range over which power-law and core galaxies co-exist, to explore the transition between the two types. Others were selected to extend the luminosity range of the core parameter relationships. The properties of the galaxies, such as luminosity, velocity dispersion, distance, and morphology are listed in Table 2. A set of galaxies already observed with WFPC1 and presented by Lauer et al. (1995) were also re-observed with WFPC2 when it was felt that the improved resolution and dynamic range might lead to a

significant improvement in the galaxies’ central structure. In the end, the sample is rich in core galaxies, with relatively few power-law galaxies; it thus is complementary to the Rest et al. (2001) sample, which is rich in power-law galaxies.

2.2. Images and Image Reduction

All galaxies were imaged with the high-resolution PC1 CCD in WFPC2; the image scale is $0''.0456/\text{pixel}$. Nearly all galaxies were imaged in the F555W filter (equivalent to broad band V); images were also obtained in F814W filter (broad band I) to provide color information for many galaxies. The exposure time for most galaxies was roughly a single orbit in each filter, typically split into several sub-exposures to allow for cosmic-ray event repair. The exposure levels in the galaxy centers varied widely over the sample, but were typically $> 10^4 e^-$, which is optimal for point-spread function (PSF) deconvolution.

Beginning in program G0 6587, many of the image sets were dithered in a 2×2 square pattern of 0.5 PC pixel substeps. This procedure allows for the removal of the aliasing present in any single PC image and consequent recovery of the optimal spatial resolution provided by the $HST+WFPC2$ combination. The reduction procedure for a given image set depended on whether the images were dithered. Non-dithered image sets were always obtained with the same pointing and could simply be compared to detect and repair cosmic-ray events, before being stacked.

The dithered images for a given galaxy and filter combination were combined into a single Nyquist-sampled “super-image” using the Fourier algorithm presented by Lauer (1999a). The algorithm combines the images in the Fourier domain and is designed to recover the Nyquist image even if the dither positions are somewhat non-optimal. The output of the algorithm is a double-sampled image with 0.5 PC pixel steps. The Fourier algorithm is theoretically justified and introduces no blurring of the data; this is in contrast to *Drizzle* (Fruchter & Hook 2002), which cannot remove aliasing in a small dataset, and introduces additional blurring on the scale of the original pixel sampling. A drawback of our reduction path is that the pointing of each image in the image-set is slightly different, complicating the repair of cosmic-ray events.³ The procedure used for cosmic ray repair was to first intercompare the images ignoring their small offsets and then construct a Nyquist image from the repaired images. This first estimate of the Nyquist image was used to improve the initial detection of the cosmic-ray events, thus producing a revised Nyquist image. This procedure was iterated a second time to produce the final image.

The final step was to deconvolve the PSF. The $HST+WFPC2$ PSF introduces significant blurring as far as $0''.5$ from the galaxy centers, but deconvolution can recover the intrinsic surface brightness profiles to a few percent accuracy for $r \geq 0''.04$ (Lauer et al. 1998). Deconvolution was

³This is not a difficulty intrinsic to dithering. With an additional orbit’s worth of exposure time, redundant exposures could be obtained at each dither position.

achieved by 40 iterations of the Lucy-Richardson (Lucy 1974; Richardson 1972) algorithm. The PSFs were calculated from the Tiny-Tim package (Krist 1995). For the double-sampled images, the Tiny-Tim PSFs were convolved with the pixel-response function of Lauer (1999b).

2.3. Surface Photometry

Central images of the sample galaxies are shown in Figures 1 and 2. While the classic view of early-type galaxies is that they are purely stellar systems with elliptical isophotes, the majority of the galaxies depart from this picture one way or another, having central dust patches or rings, stellar disks, nuclear clusters, central minima, and so on. A summary of the morphological features seen is presented in Table 3. Figure 1 also shows the galaxy images divided by models reconstructed from the surface photometry (described below) to help isolate these features. Those galaxies that had their centers so obscured by dust that surface photometry could not be derived are shown separately in Figure 2. The overall importance of dust for any galaxy was roughly quantified by comparing the integrated light of the observations to model galaxy images reconstructed from the surface photometry within $1''$ of the galaxy centers. The dust absorption thus estimated is presented in Table 3 in units of hundredths of a magnitude. These absorption values are not intended for quantitative astrophysical interpretation, but do seem to correspond well to subjective impressions of the strength of central dust seen in Figure 1.

Surface photometry was derived under the assumption that the isophotes are concentric ellipses, but with position angle and ellipticity that can vary arbitrarily with radius. The photometry was measured in several stages. The first step was to mask obvious stars, dust patches, image defects, and so on, from the images. Initial photometry was derived using the least-squares algorithm of Lauer (1986). A model reconstructed from photometry was then subtracted from the images to isolate and mask more subtle features that were missed during the initial pass. For galaxies with extensive dust this procedure was often iterated several times, as the isophote parameters would often change significantly as the mask was refined. The final stage was to measure the inner isophotes ($r < 0''.5$) with the high-resolution algorithm of Lauer (1985). This algorithm uses sinc-interpolation to sample the image, thus preserving the spatial resolution of the images. For this stage, image defects were initially filled in with a model constructed from the lower-resolution photometry, and then with a model constructed from the high-resolution photometry.

The final surface photometry profiles are presented in Figure 3⁴. The zeropoint calibration was obtained from Holtzman et al. (1995). A “sky” level for each galaxy was measured from the corner of the WFPC2 WF3 CCD farthest away from the galaxy center (typically $1'.8$ in angle), and was subtracted from the photometry. For the more extended galaxies, the sky will have some galaxy-

⁴Tabulated versions of the photometry are presented in the electronic version of this paper, and at <http://www.noao.edu/noao/staff/lauer/nuker.html>.

light contamination, but given that the present study focuses on the brighter central isophotes, this will cause only a small error.

2.4. WFPC1 versus WFPC2 Photometry

A number of galaxies in the sample were originally observed with WFPC1. The new WFPC2 photometry allows a test of the WFPC1 observations, which required large deconvolution corrections. Figure 4 compares WFPC2 and WFPC1 profiles for several galaxies. Lauer et al. (1993) argued based on simulations that deconvolution could recover profiles from WFPC1 that were accurate to a few percent for $r > 0''.1$, with significant residual blurring at smaller radii. The comparison of WFPC2 and WFPC1 photometry for M32 and M33 presented by Lauer et al. (1998) showed this conclusion to be essentially correct, while underscoring the need to deconvolve WFPC2 photometry as well. Figure 4 ratifies this conclusion for a larger set of galaxies. For the most part, the WFPC2 and WFPC1 profiles agree extremely well for $r > 0''.1$. The exception to this general rule appears to be galaxies with strong nuclei, such as NGC 3115, where light from the central point-source spilled beyond $r \approx 0''.1$, and was poorly recovered by WFPC1. Weak nuclei in core galaxies, such as in NGC 1399, were also poorly captured by WFPC1. The conclusion, overall, is that the WFPC1 profiles can still be used to their stated $0''.1$ resolution limit.

3. Nuker Law Fits

We fitted the surface brightness profiles with the “Nuker law” (Lauer et al. 1995) parametric form

$$I(r) = 2^{(\beta-\gamma)/\alpha} I_b \left(\frac{r_b}{r}\right)^\gamma \left[1 + \left(\frac{r}{r_b}\right)^\alpha\right]^{(\gamma-\beta)/\alpha}, \quad (1)$$

which describes the profiles as a “broken power law;” it is an extension of a broken power-law form first used to describe the brightness profile of M32 (Lauer et al. 1992b). Here r is the semi-major axis⁵. The outer portion of the profile is a steep power-law with logarithmic slope, $-\beta$. This outer power-law “breaks” at radius r_b , transitioning to a shallower inner power-law with slope $-\gamma$. The smoothness or “speed” of transition is determined by α ; the intensity scale is set by I_b , the surface brightness at r_b . The break radius is both the point of maximum curvature of the profile in logarithmic coordinates and the location where the local slope is the average, $-(\beta + \gamma)/2$, of the inner and outer slopes. In passing, we note that we are aware of the limitations of parametric fits to data. However, a nonparametric analysis of the WFPC1 profiles by Gebhardt et al. (1996) yielded no additional insight into the central structure of elliptical galaxies than was provided by the parametric analysis of Lauer et al. (1995) and Faber et al. (1997) using the Nuker law.

⁵This differs from Byun et al. (1996) where r represented the geometric mean of the semi-major and semi-minor axes.

We fitted the major-axis profiles using the MINUIT package (James & Roos 1977), which was also used by Byun et al. (1996) to fit the WFPC1 profiles. Unlike Byun et al., however, we allowed the algorithm to find solutions with $\gamma < 0$; the discovery of galaxies with central *minima* in surface brightness (Lauer et al. 2002) shows that central brightness profiles with positive slopes must be allowed for. While in formally $\gamma < 0$ would imply that the surface brightness profile goes to zero as $r \rightarrow 0$, which is impossible in projection, the integrated brightness in any aperture remains positive, and more to the point, we mean to imply no behavior of the profile within the resolution limit. The Nuker law parameters for all galaxies in Figure 1 are listed in Table 4 and plotted in Figure 3. The radial domain fitted was adjusted on an *ad hoc* basis based on the structure of a given galaxy and the residuals of an initial Nuker law fit over the entire extent of the profile. Typically an inner limit was specified to avoid nuclei (see below), which the Nuker law is not intended to represent. An outer limit was specified in some cases to avoid deviations from the Nuker law that might have influenced the quality of the fit to the inner region. The fits are shown as solid lines in Figure 3, with the extent of the line showing the radial range of the fit. The fit residuals are plotted at the bottom of the brightness profile panels.

Lauer et al. (1995) showed that the brightness profiles could be grouped into two classes. “Core galaxies” show an obvious break in logarithmic slope that marks a transition to a shallow inner cusp with $\gamma' < 0.3$, where γ' is the slope at the *HST* resolution limit ($0''.04$ for the F555W WFPC2 images). “Power-law galaxies,” in contrast, retain a steep slope, $\gamma' > 0.5$, into the resolution limit. As was shown by Gebhardt et al. (1996) and Faber et al. (1997), the distribution of cusp slopes is bimodal, with no examples of galaxies in those papers with $0.3 < \gamma' < 0.5$. This classification scheme will be re-examined in detail in Paper VI. The adopted profile classifications are listed in Table 4. In some cases, as noted in Table 4, we have reclassified a number of galaxies previously observed by ourselves or others because we have adopted finer resolution limits or used higher resolution imagery than the previous investigations.

Rest et al. (2001) and Ravindranath et al. (2001) identified a set of galaxies that have $0.3 < \gamma' < 0.5$, which Rest et al. call “intermediate” galaxies. Three such galaxies (NGC 821, 3585, and 7723) are in the present sample. As Ravindranath et al. (2001) showed, intermediate types are rare, so that the distribution of cusp slopes remains bimodal, even if the region between core and power-law galaxies is no longer completely empty. We also validate the concern of Rest et al. (2001) that the intermediate classification is highly sensitive to resolution. As it happens, after adopting finer resolution limits than did Rest et al., we consider *all* of their intermediate galaxies to be core galaxies, while we now consider some of their power-law galaxies to be intermediates. We will explore this issue in detail in Paper VI.

4. The Central Structure of Early-Type Galaxies

4.1. Inner Isophote Ellipticity and Central Stellar Disks

Figure 5 plots the average isophote ellipticity interior to r_b , weighted by the integrated isophote luminosity (analogous to equation (2) in §4.2 below), as a function of the average exterior ellipticity (averaged the same way but for $r > r_b$) for both core and power-law galaxies (ellipticity values are given in Table 5). There is no clear trend for either type of galaxy to become systematically flatter or rounder as the center is approached. What is evident in Figure 5, however, is that the power-law galaxies on average are more elliptical than core galaxies. This trend is also seen in Figure 6, which plots inner ellipticity as a function of galaxy luminosity. While Vincent & Ryden (2005) show that elliptical galaxies overall become rounder with increasing luminosity, and cores become more prevalent with luminosity, core galaxies are rounder than power-law galaxies at the same luminosity. Ryden et al. (2001) looked at *HST* photometry of a large sample of elliptical galaxies and reached similar conclusions. In particular, they looked at isophote shape as a function of the fractional distance to the effective radius, finding that the distinction between core and power-law galaxies was strongest at the smallest radii.

Jaffe et al. (1994) and Ferrarese et al. (1994) noted that the power-law galaxies (their Type II) in their sample were highly elliptical, while the core galaxies (their Type I) were nearly round. They argued that the difference between the two was *merely one of projection*. In their view, all ellipticals harbored disks, which when seen edge-on would make sharply rising cusps; the stellar density profiles of all ellipticals would have essentially the same form. Lauer et al. (1995) disagreed with this picture, noting the existence of round power-law galaxies, which should not exist at all in the projection model. Moreover, the new data in Figures 5 and 6 show that core galaxies co-exist with power-law galaxies at all ellipticities. Although core galaxies are on average rounder than power-law galaxies, the ellipticity distributions of the two types overlap significantly, whereas the projection model implies a much cleaner separation.

Lauer (1985) also claimed that the majority of highly elliptical power-law galaxies showed no evidence of a central stellar disk; however, we now think that such cases are rare. First Faber et al. (1997) subsequently noted that power-law galaxies have disk-like *outer* isophotes, which firmly associates power-laws with disks. Now, new WFPC2 imagery here shows that disks can be seen in *nearly all* power-law galaxies with inner ellipticity $\epsilon \geq 0.3$, whereas *no* disks are seen in power-law galaxies rounder than that (see Figure 6). This strong dichotomy suggests that *all* power-law galaxies harbor disks; their visibility is simply due to the viewing angle. It is true that Lauer et al. (1995) found disks in only three out of nine highly elliptical power-law galaxies; however, some of the disks in the present sample are faint and may have been poorly visible in WFPC1 imagery. While, in common with Lauer et al. (1995), we cannot detect a disk in the power-law galaxy NGC 1426 (which has $\epsilon = 0.32$), we do find a disk in NGC 4458 (and now classify it as a core rather than power-law galaxy).

Core galaxies generally have boxy isophotes (Faber et al. 1997), but we find disks in four core galaxies, all of which have high inner $\epsilon \geq 0.3$. Three of these are rather dim, having $M_V > -21$, and only one (NGC 3706) of the five highly elliptical core galaxies brighter than this has a disk. Two of the three intermediate galaxies also have disks, and they also lie in the same magnitude transition zone near $M_V \sim -21$.

The overall impression is that disks are frequent if not ubiquitous in power-law galaxies, populate a fair fraction of faint cores and intermediate galaxies in the transition zone, and then peter out amongst bright core galaxies. The disappearance of disks with brightness seems to be related to the core/power-law transition itself and may give a clue as to how it occurs, as discussed in the summary.

4.2. Isophote Twists in the Inner Profiles

An examination of the isophote position angle profiles presented in Figure 3 shows that many core galaxies have significant isophote twists close to or interior to their break radii. This behavior, for example, can be seen in NGC 507, the first galaxy presented in Figure 3. The general phenomenon is that most core galaxies have isophote orientations that remain essentially constant over their outer radii (within the regions imaged by WFPC2), but at some small radius the isophotes smoothly twist away from the outer orientations.

To quantify this phenomenon, we fitted the position angle profiles of the core galaxies with a “hinged” line. In detail, a line was first fitted over the outer portion of the profile, starting at an inner limiting “hinge” radius. Once the parameters of the outer line were determined, a second line was fitted interior to the hinge radius (but still with $r > 0''.13$ to avoid nuclei) with the constraint that the inner line had to intersect with the outer line at the hinge radius. The effect is to fit the entire position angle profile with two lines of differing slope that intersect at a “hinge.” The position of the hinge was selected by finding the location that minimized the residuals of the entire position angle profile fitted by both line segments. The final fits are shown as dotted lines in the position angle plots in Figure 3.

Table 8 presents the values of the inner and outer position angle gradients, the hinge radius, and the local logarithmic slope of the brightness profile, γ' , at that location. Figure 7 shows the inner position angle gradients as a function of γ' at the transition radius. The symbols plotted also show the inner and outer gradients schematically as angled wedges, with the slopes of the segments to the left and right of the vertex proportional to the inner and outer position-angle gradients. Both the table and figure show that the isophote position angle varies only slowly outside the hinge radius, but strong twists occur at small radii. The transition in behavior occurs near $\gamma' \approx 0.5$, a point typically within the shallow surface brightness cusp interior to the core break-radius.

Figure 8 plots the same data for the power-law galaxies. The power-law galaxies appear to have at most very small twists in their inner isophotes. Only two galaxies not affected by dust

have gradients that exceed $30^\circ/(\Delta \log(r) = 1)$. Consideration of the true “power” in the twists in power law galaxies, however, suggests that they are as significant as the large twists seen in the inner cusps of the core galaxies. The significance of any given isophote twist is tied to how much the light distribution in a galaxy must have changed to exhibit the twist. Very little light needs to be redistributed in a portion of a galaxy with a shallow brightness gradient and nearly circular isophotes to cause a strong twist in angle, while the perturbation must be large when the gradient is steep or the isophotes are highly elliptical.

We have attempted to quantify these effects by following the general approach of Ryden et al. (1999), who analyzed the shapes of dwarf ellipticals by introducing a twist-measure that accounts for the true perturbation in the projected light distribution of a galaxy to produce the observed twists. The basic concept is to measure the relative amount of light required to “iron-out” or untwist a twisted galaxy. The first step is to use the brightness profiles to calculate the luminosity-weighted average position angle of a given galaxy,

$$\langle \phi \rangle = \frac{1}{L(r_1, r_2)} \int_{r_1}^{r_2} \phi(r) \Sigma(r) dA, \quad (2)$$

over a major-axis range $r_1 < r < r_2$ in which the twist is to be measured. Here $\phi(r)$ gives the isophote position angle profile, $\Sigma(r)$ is the brightness profile, $L(r_1, r_2) = \int_{r_1}^{r_2} \Sigma(r) dA$ is the integrated galaxy luminosity over the radial range, and the area element is

$$dA = 2\pi q r \left(1 + \frac{1}{2} \frac{d \ln q}{d \ln r} \right) dr, \quad (3)$$

where $q = 1 - \epsilon$, the ratio of isophote minor to major axes at r . The “surface-brightness twist” is estimated as

$$T = \left(\frac{1}{N} \sum \left(\frac{I_{\langle \phi \rangle}(x, y) - I(x, y)}{I(x, y)} \right)^2 \right)^{1/2}, \quad (4)$$

where $I_{\langle \phi \rangle}(x, y)$ is an image reconstructed from the surface photometry with the isophotes all forced to have position angle $\langle \phi \rangle$, while $I(x, y)$ is an image reconstructed from the surface photometry with the twists as measured⁶, and the sum is over the N pixels within $r_1 < r < r_2$. The surface-brightness twist thus is a typical relative root-mean-square (rms) measure of the difference between the untwisted and observed galaxy. We emphasize that our T measure differs from that of Ryden et al. (1999), which we believe suffers from a conceptual error in its derivation.

We have calculated surface-brightness twists separately for the radius ranges inside and outside the hinge radius (limited to an outer radius three times larger than the hinge-radius defining the boundary of the inner and outer gradients); they are presented in Table 8 and Figure 9. As can be seen, both power-law and core galaxies exhibit somewhat stronger twists in their inner regions. The inner-twists are typically $\sim 3\times$ stronger for both types of galaxies than the outer twists. Displayed

⁶Both reconstructions assume concentric elliptical isophotes and allow the ellipticity to vary with radius.

this way, however, we see that the significance of the inner twists in both core and power-law galaxies is essentially the same.

4.3. Central Color Gradients

The $V - I$ color gradients of the inner regions of the sample galaxies are generically similar to those seen farther out in the envelopes of early-type galaxies. The great majority of sample galaxies become slightly redder toward the center. The exceptions are NGC 2300, 4382, and 7457, which have shallow gradients that become *bluer* with decreasing radius. As seen in Figure 3, the color gradients are roughly linear with shallow slopes in logarithmic coordinates. Table 7 lists the color gradients measured over $0''.2 < r < 10''$; the inner cutoff is set to avoid nuclear sources. Figure 4 of Carollo et al. (1997) suggests that the color gradients show more variability over $0''.25 < r < 1''.5$ than they do at larger radii, but we do not see this effect.

The strengths of the color gradients superficially appear to depend on the profile type of the galaxy, as already suggested by Figure 11 of Carollo et al. (1997), and by high-resolution ground-based images of galaxy centers (Michard 1998); however, this effect appears largely to be due to the greater prevalence of dust in power-law galaxies. Figure 10 plots the color gradients as a function of the limiting logarithmic profile slope at the resolution limit, γ' ; the symbol type encodes the central dust indices given in Table 3, with open symbols corresponding to galaxies with dust absorption greater than 0.02 mag. Even though we attempted to exclude visible dust patches from the profile estimation algorithms, the strongest color gradients correlate with the largest scatter about the mean gradient line, supporting the conclusion that the color profiles in these cases are still affected by residual dust absorption and are not likely to reflect true changes in the underlying stellar population. If dusty galaxies are ignored, there is still a suggestion of a weak trend for power-law galaxies to have stronger gradients than core galaxies; the mean $V - I$ gradients for the two types are -0.045 ± 0.005 mag (excluding the one power-law galaxy with a positive gradient) and -0.031 ± 0.006 mag, respectively. Clearly, however, the scatter in color gradients at any γ' is substantially larger than the small offset between the two types, and to first order both types of galaxies have essentially the same inner color gradients. Lastly, Figure 11 shows that there is no relationship between the strength of the gradient and galaxy luminosity, once dusty galaxies are excluded.

We also examined the color gradients of core galaxies to see if the gradients were smaller interior to the break radius. Because the envelope color gradients in core galaxies are small to begin with, such a change in absolute terms will be a small effect, and indeed for the majority of core galaxies it is difficult to see any change in the gradient associated with the core. However, NGC 3379, 3608, 4291, 4365, 4406, and 7619 do appear to have flatter color gradients for $r < r_b$; NGC 4406 provides the best example, but the significance of this effect is low.

4.4. Nuclei

A substantial fraction of the sample galaxies have nuclei, a compact light source that is seen to rise above the inward extrapolated surface brightness cusp at small radii. In the present sample we find 13/45 (29%) of the core galaxies and 12/20 (60%) of the power-law galaxies to have nuclei. Nuclei were recognized by visual inspection of the residuals of the Nuker law fits to the surface brightness profiles. For the fainter nuclei in core galaxies, the inner radial limits of the fits were often increased to better isolate nuclei included in the initial fits.

Table 6 lists the luminosities and colors of the nuclei identified. The luminosities were derived by integrating the central residuals from the Nuker law fits. This procedure presumes that the Nuker law can be extrapolated inwards from the radial domain over which the fit was performed. The total fluxes of the nuclei may thus have unknown systematic errors. At the same time, our nuclear luminosities for NGC 4278, 4365, and 4552 agree extremely well with those of Carollo et al. (1997). The color of the nucleus is that of the central light source isolated from the hosting galaxy; it is estimated from the Nuker law residuals in the V band and the $V - I$ profiles on the assumption that the $V - I$ color just outside the nuclei gives the color of the background starlight. The colors have been corrected for Galactic reddening. The $\Delta(V - I)$ colors listed in Table 6 give the change in color of the nuclei relative to these fiducial values. Note that a faint nucleus associated with a significant decrease in the central total $V - I$ will thus be inferred to be extremely blue.

In general the nuclei are bluer than the background galaxy starlight immediately outside the nuclei, although they are not particularly blue in absolute terms. Most nuclei are also spatially unresolved (more compact than ~ 5 pc); only the nuclei in NGC 741 and 4365 appear to be resolved with scales of ~ 20 pc and ~ 10 pc, respectively⁷. If the nuclei are star clusters, then they may comprise stars younger or more metal-poor than those in the host galaxies. We note that most of the nuclei are too luminous to be classic globular clusters. A better analog in color, luminosity, and physical compactness would be the M33 nuclear star cluster (Lauer et al. 1998). In passing, we note that NGC 5419 appears to have a double point source at its center. The brighter component is at the photocenter of the galaxy; the second component appears to be weakly resolved.

The detection of nuclei in many power-law galaxies is not surprising in light of previous work. Lauer et al. (1995) identified nuclei in a large fraction of their power-law galaxies (some of which are in the present sample); Rest et al. (2001) also found nuclei in a number of power-law galaxies. The frequency of nuclei in core galaxies is less well understood. Lauer et al. (1995) found nuclei in only two of their core galaxies, NGC 6166, and the brightest cluster galaxy (BCG) in A2052, both of which were known to be AGN. However, the WFPC1 images were poorly suited to detecting faint nuclei. Carollo et al. (1997) were the first to use WFPC2 for this problem; they only observed a few core galaxies, but found nuclei in most of them. Rest et al. (2001) also used WFPC2, but found nuclei in only one of their nine core galaxies. Ravindranath et al. (2001) found nuclei in 5/13 of

⁷Carollo et al. (1997) noted the resolved extent of the NGC 4365 nucleus, as well.

their core galaxies, consistent with the present detection rate. Rest et al. adopted very conservative criteria for identifying nuclei, while Ravindranath et al. always included a nuclear point source in their Nuker law fits. Lastly, Laine et al. (2002) detected nuclei in $\approx 15\%$ of their BCG sample, which mainly had core galaxies. The BCG are in general at much larger distances than the galaxies in the present sample and observed in the I band, both making the detection of nuclei difficult. The present sample is also rich in core galaxies, and the 29% detection rate is probably a more representative number than in previous samples.

There is too little information to determine whether nuclei are star clusters or are AGNs; both phenomena are probably present. Ravindranath et al. (2001) argued that at least 11/14 of their nuclei were associated with AGN. In the present sample AGN are likely to explain NGC 1316 (Fabbiano et al. 1994), 4552 (Cappellari et al. 1999), and 7457 (Gebhardt et al. 2003). Table 3 lists what is known about nuclear activity of the sample galaxies based on the optical emission lines. There is weak evidence that power-law galaxies with nuclei have absorption-line spectra, while core galaxies with nuclei have strong emission lines. However, exceptions in both directions exist; in particular, a number of core galaxies with emission lines showed no nuclei in the present surface photometry. We thus cannot conclude that low-level AGN, even if present, explain the all nuclear sources seen in the broad-band *HST* images.

4.5. Galaxies with Central Minima

A basic structural paradigm that underlies the present structural analysis of early type galaxies is that their central starlight distributions can be described by concentric elliptical isophotes with surface brightness increasing monotonically towards the center. There is however, an increasingly large set of objects that depart from this picture. M31 (Lauer et al. 1993) and NGC4486B (Lauer et al. 1996) have double nuclei, and Lauer et al. (2002) identify a number of galaxies that have local *minima* in their brightness profiles at or near their centers. In this section we discuss NGC 4073 and 4382, which also have central surface brightness minima. In the next section we discuss an additional set of galaxies in which the location of maximum brightness within the core is spatially offset from the photocenter of the core itself.

We speculate that a substantial majority if not all of these systems may be cases where black holes were critical to either creating or preserving the unusual structures over long times. Tremaine (1995), for example, explains the double nuclei in M31 (and by implication, NGC 4486B) as the projected appearance of an eccentric disk of starlight stabilized by a central black hole. In the case of the galaxies with central minima, Lauer et al. (2002) advanced two competing explanations for the creation of such systems, both involving black holes. The first is that a diffuse torus of starlight has been added to a pre-existing core to create the appearance of a central minimum interior to the torus. This would occur during the final stages of merging in which the tidal field of the black hole in the more massive galaxy disrupts the dense center of a galaxy being cannibalized (Holley-Bockelmann & Richstone 2000). A second, more exotic idea is that stars have actually been ejected

from the galaxy center by the decay of a central black hole binary created in a merger.

Lauer et al. (2002) further noted that at least some of galaxies with central minima may be related to the double nucleus systems. Strictly speaking, M31 and NGC 4486B have locations near their centers at which a local minimum in surface brightness occurs, and could thus be included in the class of galaxies with central minima. Conversely, the local minima in some of the Lauer et al. (2002) galaxies are bracketed by structures that create the appearance of highly diffuse double nuclei. Separately, the central minimum in NGC 3706 is clearly due to a well defined central ring of stars that might create a double nucleus if it were slightly more eccentric or were viewed from a different angle; the central structure in NGC 3706 resembles that of M31 in other ways. In the present sample, the center of NGC 4073 resembles that of Lauer et al. (2002) galaxies NGC 4406 and 6876, while NGC 4382 is yet another galaxy with a central minimum that resembles M31. Lastly, we note that the galaxies with offset centers, which we discuss in §4.6, may be poorly resolved examples of double nuclei or galaxies with central minima.

4.5.1. NGC 4073

The core galaxy NGC 4073 is the brightest galaxy in the poor cluster MKW4; it is likely to have cannibalized other cluster members. Fisher et al. (1995) obtained a rotation curve and stellar velocity dispersion profile. The central few arcseconds of the kinematic profiles reveal a $\sim 10\%$ depression in velocity dispersion and counter-rotation. Fisher et al. (1995) thus argue that NGC 4073 has a kinematically-decoupled core.

The envelope of NGC 4073 has a fairly high ellipticity of 0.4; however, for $r < 5''$, the isophotes rapidly become nearly circular and show a strong twist of over 90° , as is evident in the profiles shown in Figure 3, and in a contour plot of the galaxy center (Figure 12). The maximum surface brightness is reached in a “ring” at $r \approx 0''.16$, with the brightness falling by 0.14 mag at the center of the galaxy. At larger radii the surface brightness profile (Figure 3) first *increases* in slope with decreasing radius for $r < 1''$, before abruptly flattening off just outside the ring. Superficially, a high contrast image of the galaxy center (Figure 13, left) suggests that the center is obscured by a dust patch; however, an archival NICMOS-2 image (Figure 13, right) (GTO 7820) in the H band also shows a central minimum, despite its lower angular resolution. We conclude that we are seeing the intrinsic distribution of starlight rather than obscuration.

A close examination of the image and contour plot shows that the central ring is not exactly symmetric, but is slightly brighter to one side. A cut through the center at position angle 166° shows this clearly (Figure 14) by going through the brightest part of the ring. The maximum brightness along the cut occurs at $0''.18$ from the central minimum, slightly further away from the center than the diametrically-opposed maximum, which occurs at $0''.15$ from the central minimum. The implied eccentricity of the ring is $e \sim 0.07$. The slightly asymmetric brightness distribution could be explained by an eccentric torus of stars (Tremaine 1995). However, the ring-radius corresponds

to ~ 70 pc, a considerably larger scale than that of the central minima discussed in Lauer et al. (2002), and one that is outside the nominal ≈ 30 pc sphere-of-influence of a central black hole based on the velocity dispersion of NGC 4073 (Table 2) and the Tremaine et al. (2002) $M_{\bullet} - \sigma$ relationship. If so, the stability of such a torus might therefore be in question.

4.5.2. NGC 4382

The central structure of NGC 4382, a bright S0 core galaxy in the Virgo cluster, somewhat resembles the double nucleus of M31; here the central minimum is a “valley” between two brightness peaks. This might result from the projected appearance of a much more eccentric torus or stellar disk than that seen in NGC 4073. As can be seen in Figures 15 and 16 the isophotes become asymmetric for $r < 0''.5$, rounding out and becoming somewhat diffuse at position angle $\sim 40^{\circ}$. This side of the nucleus suggests a reduced-amplitude version of the off-center P1 component of M31⁸; indeed, a local surface brightness peak occurs at PA = 64° , separated by $0''.14$ from the brightest portion of the nucleus, which itself is within $0''.01$ of the galaxy envelope photocenter. Based on the velocity dispersion of NGC 4382 (Table 2) and the Tremaine et al. (2002) $M_{\bullet} - \sigma$ relationship, the estimated sphere-of-influence of a central black hole is $\approx 0''.16$. Again like M31, the isophotes become more eccentric and twist $> 20^{\circ}$ within $r \sim 1''$ as the nucleus is approached (Figure 3). The position angle of the line connecting the two brightness peaks is itself twisted away from isophotes of semimajor axes of only $\sim 0''.15$. The isophotes on the side of the photocenter opposite the secondary peak become highly eccentric, appearing as an almost linear extension of the central nucleus; this in turn resembles the P2 component of M31. Similar structure is seen in both the V and I bands; a color-ratio image (Figure 15) is flat (except for a slight radial gradient), showing no evidence for dust or change in stellar population associated with the unusual nuclear structure.

From other data, NGC 4382 appears to be an excellent candidate for a fairly recent merger; the central structure noted here may be related to the unusual spectral properties of the central regions detected from ground-based observations. NGC 4382 has the second-highest fine-structure measure in the Schweizer & Seitzer (1992) sample, who argue that the fine-structure measure is indicative of the time and strength of the last merger. Fisher et al. (1996) obtained long-slit line-strength measures over the central region of NGC 4382, finding it to have an exceptionally large $H\beta$ absorption line-width of 2.6\AA ; they argued that the central population of NGC 4382 is as young as 3 Gyr. They also confirm that the galaxy becomes steadily *bluer* with decreasing radius for $r > 4''$, as was first noted by Bender & Möllenhoff (1987). The present $V - I$ color profile of NGC 4382 also shows a centrally blue gradient for $r < 10''$; as discussed in §4.3, nearly all galaxies have $V - I$

⁸P1 is the brighter, more diffuse component of the M31 nucleus in the optical. P2 is the less luminous peak, but it marks the center of the galaxy and the location of the M31 nuclear black hole. See Lauer et al. (1993) or Lauer et al. (1998) for details.

color gradients that become redder at small radii. We also note that NGC 4382 has an average $V - I$ color that is bluer than all but one galaxy in the present sample (Table 7). We do, however, disagree with some of the finer details of the NGC 4382 color distribution presented by Fisher et al. (1996) — we find that the nucleus is essentially the same color as the surrounding galaxy for $r < 10''$, and we do not find any evidence for a central ring of particularly blue emission. Fisher (1997) notes that the stellar velocity dispersion profile of NGC 4382 decreases for $r < 5''$, which is confirmed in SAURON observations (Emsellem et al. 2004). High spatial-resolution spectroscopy with the OASIS instrument shows that the core within $r < 2''$ counter-rotates with respect to the outer envelope of the galaxy (McDermid et al. 2004).

4.6. Galaxies with Offset Centers

In our data, the location of maximum surface brightness is typically concentric with the surrounding galaxy, as measured by the center of the isophotes on $\sim 1''$ scales, with a median precision of $0''.005$; 75% of the sample has the peak brightness concentric to within $0''.01$. In physical units, this means that the galaxy centers are aligned at the sub-parsec level with the isophotes on the scale of the break radii farther out. Any lopsidedness or strong $m = 1$ asymmetries on the scale of the galaxy cores is therefore extremely rare (or of extremely low amplitude). However, we identify five galaxies (Table 3) in which the center of the surface brightness cusp appears to be significantly displaced from the surrounding galaxy.

In NGC 507, the brightness peak is displaced $0''.06$ from the surrounding core; this is readily apparent in a contour plot (Figure 17) and in the residuals of the surface photometry model (Figure 1). Examination of the image of NGC 1374 shows that its brightness peak is clearly offset from its core (Figure 18), but the measured offset is only $0''.02$. The image of NGC 7619 looks normal, but the surface photometry model shows a clear pattern associated with an offset peak, which is found to be displaced from the core by $0''.04$. NGC 4291 and 5576 show similar central offsets when the model is compared to the images. In contrast, Lauer et al. (1995) identified NGC 1700 as a possible candidate for an offset center, but the improved imagery presented here shows no such effect. The five galaxies identified here with offset centers are all core galaxies, but the implied $\sim 12\%$ fraction of core galaxies with offset centers is too small to rule out similar behavior in the power-law galaxies, which are more poorly represented in the present sample.

It is now recognized that many early-type galaxies are triaxial, rather than axisymmetric. The term “triaxial” is usually taken to mean that the galaxy is symmetric with respect to three orthogonal principal planes (the D_{2h} point symmetry group); if this symmetry is present then all isophotes should be concentric. However, there is no known dynamical argument that prohibits self-consistent stellar systems without this symmetry (e.g., lopsided systems). The observation that the centers of most early-type galaxies have concentric isophotes therefore shows that some aspect of the galaxy-formation process strongly favors systems with D_{2h} symmetry. In the rare exceptions such as M31 (Lauer et al. 1998), the lopsidedness appears to be localized within the

sphere of influence of the central black hole, which is natural since orbits do not precess in a Kepler potential, so a lopsided orbit distribution is not axisymmetrized by phase mixing (e.g., Peiris & Tremaine 2003).

The coincidence of the point of maximum surface brightness with the centroid of the isophotes on larger scales also suggests that any massive black hole is located at the bottom of the potential well due to the stellar mass distribution to within a fraction of a parsec. Massive black holes are normally expected to be close to the potential minimum because they rapidly lose orbital energy due to dynamical friction; however, the black hole will execute Brownian motion relative to the potential minimum due to gravitational encounters with nearby stars. The expected rms amplitude r_{br} and velocity v_{br} of this motion have been discussed by many authors. Bahcall & Wolf (1976) argued that the black hole should be in energy equipartition with the unbound stars surrounding it; for a hole of mass M embedded in a homogeneous core with core radius r_c we then expect that $r_{br} \sim r_c(m_*/M)^{1/2}$ and $v_{br} \sim \sigma(m_*/M)^{1/2}$ where m_* is the typical stellar mass and σ is the velocity dispersion in the core. Chatterjee et al. (2002) obtained a similar result, which they confirmed using N-body simulations. However, these results are for galaxies with homogeneous cores, not the singular density distributions that are found in both core and power-law galaxies. There has been very little theoretical work on the expected value of r_{br} in galaxies with cusps.⁹ However, it is likely that the formula for a homogeneous core provides an approximate upper limit to r_b in a singular core, when the core radius of the homogeneous core is replaced by the break radius of the singular core. For characteristic values $r_c \sim 100\text{pc}$ and $M \sim 10^8 M_\odot$ we find $r_{br} \sim 0.01\text{pc}$, too small to be resolved by *HST*. Black holes in a binary may also be displaced from the center. The expected binary semi-major axes are in the range 0.01 – 10 pc (Yu 2002); binaries at the larger end of this range may be within the resolution limit of *HST*.

The conclusion that Brownian wandering of a central black hole is not responsible for the offset centers leaves us with the hypothesis that these galaxies may be unresolved analogs to M31; this is suggested by the highly local nature of the offset centers plus the increasingly rich sample of early-type galaxies that have complex central structure. Nieto et al. (1986) noted that the M31 nucleus was displaced from the M31 bulge based on ground-based observations, which had ~ 1 pc limiting resolution, prior to the *HST* discovery of the complex nuclear morphology (Lauer et al. 1993). If M31 were at the distance of Virgo, its double nucleus would remain unresolved by *HST*, and would look like an off-center galaxy. The estimated sizes of the black hole sphere-of-influence range from $0''.11$ for NGC 5576 to $0''.28$ for NGC 4291, significantly larger than the observed central offsets for all five galaxies. The structure of these galaxies is thus not inconsistent with the Tremaine (1995) model for M31.

⁹Laun & Merritt (2004) provide formulae for v_{br} in the case where the galaxy density profile is a power law, but do not discuss r_b .

5. Dust in the Centers of Early-Type Galaxies

5.1. The Phenomenology of Central Dust

5.1.1. Overall Dust Frequency

It is already well-established that dust features are common in *HST* images of the centers of early type galaxies (Ferrarese et al. 1994; Jaffe et al. 1994; van den Bosch et al. 1994; van Dokkum & Franx 1995; Lauer et al. 1995; Carollo et al. 1997; Ferrari et al. 1999; Tomita et al. 2000; Tran et al. 2001). In our own sample, dust is visible in 38 out of 77 galaxies. This frequency of 49% agrees well with that of previous studies (Sadler & Gerhard 1985: 40%; Véron-Cetty & Véron 1988: 23%; Goudfrooij et al. 1994a: 41%; van Dokkum & Franx 1995: 48%; Ferrari et al. 1999: 75%; Tomita et al. 2000: 56%; Tran et al. 2001: 43% (their unbiased sample)). If we combine the samples of Tran et al. (2001) and Lauer et al. (1995) with the present sample (this combination largely encompasses all *HST* samples), we find the overall frequency of dust to be 47% in a total of 177 galaxies (see Table 9 for details). The sample of Lauer et al. (1995) avoided known dust, whereas one quarter of the Tran et al. (2001) sample was strongly biased toward it; the present sample has no obvious biases for dust. The combined sample is large enough that the observed dust fraction should approach a representative value for bright ellipticals. Dust is about equally prevalent in both power-law galaxies and cores; this agrees with frequencies seen in Tran et al. (2001) and Lauer et al. (1995).

5.1.2. Dust Morphology and Radial Distribution

Dust morphologies were determined by eye using the 4'' postage stamps shown in Figure 1. We should clarify that by “dust” in this paper we always mean clumpy dust that is visible as dark patches in *HST* images. A diffuse (and possibly more massive) warm dust component may also be present, detected by IRAS (e.g. Knapp et al. 1989, Goudfrooij & de Jong 1995, Tran et al. 2001), but that is not the focus here.

Following Tran et al. (2001), we distinguish nuclear rings and disks (which we lump together as “rings”) from all other structures (termed “non-rings”). Ring structures are presumably highly flattened, circular, and axi-symmetric (Verdoes Kleijn & de Zeeuw 2005), implying ages that are at least a few orbital times (an orbital time at 100 pc is a few million years). The non-ring class is further sub-divided into “spirals” (with sheared dust patterns), and “chaotics” (random blobs). A handful of transitional cases lie between the rings and non-rings. This schema is motivated by the notion that we are seeing various stages of a “settling sequence” (e.g., Tran et al. 2001; Verdoes Kleijn & de Zeeuw 2005). This idea is discussed further below, but it rests heavily on the fact that non-ring dust *must* be in a dynamically short-lived configuration. The settling hypothesis says that it is falling into the center to form nuclear rings.

The most striking result of the dust morphology census is that the ratio of rings to non-rings is only 0.6, consistent across all three sub-samples. This small ratio surprised us; if rings are the descendants of short-lived non-rings, we expected to find a much larger ratio of rings to non-rings. In fact, the opposite is true. We return to this point below.

We studied larger model-subtracted images covering most of the PC1 CCD to learn about the radial distribution of dust beyond $2''$, which may be relevant to the settling model.¹⁰ Dust concentration was graded qualitatively, with ‘0’ meaning that the dust is highly *unconcentrated* — dust is more prevalent beyond the $4''$ postage stamp than in it, ‘1’ means that dust is visible both inside and outside of the postage stamp, and ‘2’ means that dust is seen only in the postage stamp itself. The three dust properties, strength (as already quantified in §2.3), morphology, and radial concentration, are presented in Table 3.

Only one of our 38 dusty galaxies (NGC 6876) has unconcentrated dust (concentration class 0). Thus, when dust appears in the envelope of the galaxy, it essentially always in seen in the center, too. The converse is not true. Indeed, it is striking that galaxies with nuclear rings are completely devoid of dust outside the ring: not one dust cloud is to be found in these objects beyond the ring itself!

Overall, the radial pattern of dust suggests an *episodic* settling model in which dust appears at times throughout the galaxy and then falls to the center. Galaxies with lots of dust would be near the beginning of the cycle, when dust is still widely distributed. Nuclear rings would be the endpoint of an episode, by which time the rest of the galaxy would be dust free. The fact that galaxies with weaker dust also tend to be highly concentrated (Table 3) suggests that dust is being destroyed as it sinks to the center; it falls in, leaving just a few weak shreds by the time it nears the nucleus. A possible mechanism for dust destruction is sputtering by hot X-ray gas. Survival of some but not all dust would then require that the timescale for dust destruction by sputtering be comparable to the timescale for infall. This is consistent with the dust-radiative cooling model of Mathews & Brighenti (2003) (see also Sparks et al. 1989).

5.1.3. Dust and Nuclear Optical Emission

Many papers have found positive correlations between dust and nuclear optical emission, extended optical emission, non-thermal radio activity, and far-IR dust emission (e.g., Kim 1989; Shields 1991; Goudfrooij et al. 1994a; van Dokkum & Franx 1995; Verdoes Kleijn et al. 1999; Martel et al. 1999; Tomita et al. 2000; Tran et al. 2001). We decided to explore the relationship between dust and *central* optical emission since that relation seemed particularly close (Tran et al. 2001). Optical emission-line strengths were taken from the literature (sources given in Table 3). The emission is ranked qualitatively into four grades in Table 3: 0 (no emission), 1 (weak emission),

¹⁰These larger-scale images may be viewed at <http://www.noao.edu/noao/staff/lauer/nuker.html>.

2 (strong emission), and 3 (very strong emission). Some papers measure extended emission, but most are based on spectroscopic data and thus measure only nuclear emission, which in our galaxies has line ratios characteristic of active nuclei (Seyferts and LINERs). Since extended and nuclear emission correlate well (Kim 1989; Shields 1991; Goudfrooij et al. 1994a; Macchetto et al. 1996; Caon et al. 2000), we assume that any optical emission, however weak, signifies *nuclear activity*.

The presence of dust in the inner $4''$ of our galaxies correlates remarkably well with the presence of emission: 96% of galaxies without emission lack dust, whereas 90% of galaxies with emission have at least some dust. Furthermore, the *amounts* of dust and emission also go together: mean dust strength in weak emission galaxies is only 1.09, versus 1.85 in strong-emission and very-strong-emission galaxies (see Table 10). Tran et al. (2001) also found a close connection between dust and emission, though not quite so tight as in our sample. Notably, emission strength does not appear to depend on dust morphology; as also found by Tran et al. (2001); rings and non-rings with the same dust strength have qualitatively similar emission strengths.

This connection between dust and emission is important if it is assumed, as here, that optical emission always signifies gas falling onto a black hole. It then follows that visible dust actually *shows* us gas that is about to fall onto the hole. The distribution and motions of dust become essential clues to the feeding of local AGNs, a point that was also stressed by Tran et al. (2001).

5.1.4. Dust and Galaxy Luminosity

Figure 19 plots the histograms of dusty and clean galaxies in Virgo as a function of absolute magnitude. Dust is found in roughly half the galaxies brighter than $M_V = -21$ (which is the normal frequency), whereas *all* 16 dimmer galaxies in Virgo are dust free. The probability of this happening by chance in 16 galaxies is only $\sim 1.5 \times 10^{-5}$; if the dividing line were placed at $M_V = -20$, it would still be only 2.4×10^{-4} . Either dust is intrinsically rare in faint ellipticals, or the cluster environment discourages the accumulation of dust in small galaxies. Deciding between these hypotheses is problematic since the only good selection of faint galaxies is in the Virgo cluster.

5.2. Predictions of the Dust Settling Model

The episodic settling model implies that we should to be able to identify galaxies that are in different stages of settling. A possible sequence is offered in Figure 20. The transitional objects that appear to be in the process of settling from a non-ring configuration into a ring are particularly important. Four (perhaps five) of these are in our data, two of which are shown in Figure 20. Verdoes Kleijn & de Zeeuw (2005) note similar transitional structures in radio galaxies, which they call “lanes.” Lanes are geometrically distinct from rings and are more skewed with respect to stellar principal planes, indicating transient configurations that they suggest are in the process of settling.

If all these galaxies are really parts of a sequence — non-rings, rings, to empty — then setting the lifetime of any one phase sets the lifetime of the other two phases. A good place to start is the non-ring phase. Since non-ring dust cannot be in dynamical equilibrium, a reasonable estimate of the lifetime is the local dynamical time. The orbital time at 1 kpc in a bright elliptical galaxy is $\sim 2 \times 10^7$ yr, and at the edge of a 100 pc nuclear ring is ten times shorter. Dust sputtering times (even with self-shielding) are also of order 10^{7-8} years (Mathews & Brighenti 2003), which is consistent with destruction of some fraction of the dust as it falls in. Finally, once gas falls close to a rotating disk, the timescale to settle into a principal plane of the gravitational potential is again a few orbital times (Tohline et al. 1982; Steiman-Cameron & Durisen 1988).

The ratio of rings to non-rings can now be used to estimate the lifetime of the ring phase. Since that ratio is less than unity (0.6), the nuclear rings must be even shorter-lived! Jaffe et al. (1996) model the kinematics of the nuclear ring in NGC 4261, calling attention to the high turbulent velocity near the center. This central line-broadening is a common feature of nuclear rings (e.g., NGC 7052, van den Bosch & van der Marel 1995) and may be ubiquitous. It implies high turbulent viscosity, say Jaffe et al. (1996), which causes the inner gas to flow inward and feed the black hole. Their estimated timescale for emptying out the inner ring is $\sim 10^8$ yr, not far from the timescale needed by the settling model. Finally, rings should empty from the inside out. One might therefore expect a population of “ghost” rings that are the remnants of previously filled disks; four such candidates are in our sample, two of which are exceedingly faint (NGC 741, 2778, 3379, and 3608).

A further interesting observation is the finding by Goudfrooij et al. (1994b) that dust grains are smaller in rings than in non-rings. This is consistent with the hypothesis that the grains in rings were subjected to more sputtering by the hot gas, and are therefore older.

The final step is to deduce the length of time that galaxies remain dust free, which sets the length of the whole cycle. Since half of all bright ellipticals are dust free, the length of the dust-free phase must be of order that of the dusty phase, that is, a few times $\sim 10^7$ yr, and the length of the whole cycle is only $\sim 10^8$ yr. The assumption of a settling sequence thus implies that *clumpy dust is appearing and disappearing continually in ellipticals*. This would help to understand why there seems to be little correlation between the presence of dust and merger remnants (Tran et al. 2001); merger phenomena are comparatively long-lived and would show little correlation with more rapid dust cycling. The same reason would explain why there is little correlation between mean light-weighted stellar population ages and the presence of dust (D. Forbes, private communication).

5.3. Remaining Problems for the Dust Settling Model

The “dust settling” hypothesis leaves at least three major questions unanswered. The first is the origin of the dust, whether internal (shed by stellar winds) or external (accreted from outside). We find it striking that there is not the slightest evidence, even in very dusty galaxies, for any extra starlight, either distributed in clumps throughout the galaxy or in the neighborhood of the

dust clouds themselves.¹¹ Our subtracted models should be very sensitive to clumpy starlight, yet no trace of stars is seen. Any dust accreted from the outside must therefore be essentially *star free*, which excludes small dwarf galaxies as sources, or even tidal tails. We cannot think of any plausible external sources of dust that would be completely star free.

In contrast, a known source of dust *within* the galaxies is M-star winds, which are thought to have been detected in both the mid-IR and far-IR (e.g. Knapp et al. 1989; Goudfrooij & de Jong 1995; Xilouris et al. 2004). However, this dust is injected uniformly throughout the galaxy and is not expected to clump. Perhaps there is a thermal instability that causes the hot gas to cool into clumps, bringing dust with it. A thermal instability driven by dust cooling (Mathews & Brighenti 2003) might play such a role. Finding such a mechanism would bolster the internal origin theory.

A second problem stems from the fact that the overall length for the settling cycle seems uncomfortably short, only at most a few times 10^8 yr. If true, this points strongly to an internal origin for the dust, as the dynamical infall time from the edge of a galaxy is too long, more like 1 Gyr. Yet numerous studies have revealed galaxies in which the distribution and motions of ionized gas and dust seem *unrelated* to the motions of stars, and even counter-rotate (e.g., Bertola et al. 1984, 1988; Möllenhoff & Bender 1987; Kim 1989; Forbes 1991; Goudfrooij & de Jong 1995; Bertola et al. 1995, 1998; Corsini & Bertola 1998; Caon et al. 2000; Kannappan & Fabricant 2001). These data have been widely interpreted as incontrovertible evidence for the *external* origin of dust, at least in certain key objects. We have inspected our sample to identify our best candidates for external dust origin, using the simple criteria that the dust be extended and that its distribution over the galaxy differ strongly from that of the underlying starlight. Six objects meet these criteria (NGC 1316, 2768, 4026, 4589, 5018, and 7727). Looking at them, it is indeed hard to imagine how the dust could have come from any quasi-uniform process *inside* these systems (see the large-scale model-subtracted images noted in the footnote above). Five of these objects have strong dust, and four also have strong optical emission, which would imply that strong nuclear activity is triggered by external accretion in at least these galaxies. This would be consistent with the finding that two of the strongest known LINERs (NGC 4278 and NGC 1052) have external H I clouds in their vicinity (Raimond et al. 1981; van Gorkom et al. 1986) as does NGC 5018 (Kim 1989), another AGN in our sample. On the other hand, Tran et al. (2001) searched for relationships between dust strength and external environments, finding no connection between dust and cluster versus group membership, or the distance to the nearest neighboring galaxy.

New data on the interstellar medium in ellipticals may help to solve this problem by *overturning* the old prediction that gas and star kinematics must agree. A consensus seems to be building that the hot interstellar medium (ISM) in ellipticals is highly turbulent and is being stirred periodically by nuclear activity (Enßlin & Heinz 2002; Biller et al. 2004). Stirring of the ISM would strongly perturb warm ionized gas and dust, and would explain the many examples of highly irregular,

¹¹NGC 1275 and 5128 provide the only examples that we could find where this *does* happen; neither galaxy is in our sample. Both are conventionally explained as mergers with an external gas-rich galaxy.

disorganized velocity fields that are detected in warm gas (e.g., Caon et al. 2000). Any dust and gas thrown out to the periphery of galaxies by stirring could be further perturbed by the passage of neighboring galaxies or the pressure of hot intracluster winds. In such a way, the motions of dust, gas, and stars might become strongly decoupled, giving the appearance of an external origin for clumpy gas and dust when none is required.

The most important problem with the cycling picture is a clear idea of how all the stages fit together and what drives the whole cycle. Why does dust begin to condense into clouds in the first place? Why does the black hole accrete only dust-related gas and not other gas? What stops dust from condensing? If it is feedback from the black hole, what exactly is its nature and how does it interface with dust and dust-related gas? These questions are basic to the cycling model but currently lack answers.

We conclude by highlighting the beautiful but puzzling object NGC 3607 (Figure 21). This galaxy contains a large, dusty outer disk that must be dynamically old because of its extraordinary symmetry and tightly wrapped arms. However, this outer disk appears to transition rapidly but smoothly at the center to a second gas disk that is *perpendicular* to the first and is seen nearly edge on! This inclined disk seems to be settling onto an inclined nuclear ring. How can this happen? A facile explanation would invoke external infall of gas directly into the galaxy center, yet no disturbance in the outer dust or other sign of an interaction is seen. Thanks to its many regularities but schizophrenic nature, NGC 3607 may be a Rosetta Stone that will reward further study.

6. Summary

We have examined the central structure of early-type galaxies; a component of this analysis has included searching for morphological differences between core and power-law galaxies. We conclude by summarizing what this analysis might say about the formation of central structure in the context of hierarchical merging of galaxies with central black holes; in Faber et al. (1997) we argued that cores and power-laws are different outcomes of this process. This discussion is largely speculative — while modern merger simulations are able to study the gross effects of mergers on central structure, there are few firm theoretical predictions of the phenomena considered in the analysis sections.

The picture presented by Faber et al. (1997) is that power-law galaxies were formed by a process in which central *gaseous* dissipation and attendant star formation took place, while core galaxies were generated in the mergers of galaxies largely *free of gas*. The first generation of core galaxies would be made by merging power-laws, which themselves would harbor central black holes formed in the initial collapse of the primordial galaxy. The cores were formed in the final stage of the merger when the central black holes of the merging galaxies formed a binary that ejected stars from the center as it hardened. We can distill this scenario to be simply that power-law centers are

sites of dissipation and concentration, while cores are sites of mixing and scattering.

In the case of color gradients, this picture leads us to expect power-law galaxies to have stronger gradients than core galaxies. As star formation progresses following a merger or initial collapse of gas-rich systems, the inventory of gas is simultaneously slowly depleted and centrally concentrated, while becoming increasingly metal-enriched. The stellar density profile would reflect both the concentration of gas over time and the metal-enrichment history. Merging a then gas-free power-law galaxy with a similar system would not completely erase any pre-existing color gradients, but some dilution of the gradient might be expected. Strong mixing of stars interior to the break radius associated with the formation of a core, however, might cause significant flattening of the gradient at small radii. The present data do show that power-law galaxies on average have steeper color gradients than do core galaxies, although the difference is small and the scatter about the mean gradient for both types is large. Whether or not the color gradients in core galaxies flatten further interior to the break radius is unclear. There are some core galaxies that do appear to show this effect, but the majority do not. Unfortunately, in absolute terms the envelope gradients in core galaxies are small to begin with, and it is thus especially difficult to detect even smaller gradients over a limited radial range. We conclude that color gradients are broadly consistent with the formation of cores by binary black holes with the caveat that the effects seen are modest in absolute terms.

The discovery that core galaxies twist interior to their break radii at first glance also appears to support the formation of cores by binary black holes. If the shape of the core is related to the angular momentum vector of the binary black hole, which itself may have little to do with the principal axes of the merged galaxy, then it is easy to imagine that twists occur as one transitions from the outer regions of the core into the inner region dominated by the black hole. However, our analysis shows that the absolute physical significance of the twists must also be considered. Since the inner twists of both cores and power-laws are about the same in terms of the strength of the photometric perturbation required to twist the galaxy, it is not possible to argue that the *angularly* larger twists in core galaxies are a consequence of their particular formation mechanism.

The interpretation of nuclei in early-type galaxies depends on whether the nuclei are the non-stellar emission of low-level AGN, or are star clusters of the sort seen in M33. The existence of nuclear star clusters in cores raises a few questions. In Faber et al. (1997) we argued that the survival of cores, once created, against infalling material in subsequent mergers requires the central black hole to serve as a “guardian” that tidally disrupts any dense stellar aggregates that reach the center, a notion that has been validated by N-body simulations (Holley-Bockelmann & Richstone 2000). It thus appears that nuclear star clusters cannot be pre-existing systems that have arrived at the center through dynamical friction. The likely alternative is that such nuclei were created *in situ* by the central accretion of small amounts of gas with subsequent star formation. This scenario may be supported by the bluer colors of the nuclei if they indicate that the nuclei are younger than the rest of the central stellar population. The remaining issue is to understand how converting any infalling gas into stars competes with accretion into the black hole, itself. The same problem exists

in the center of our own Galaxy, where a very young star cluster surrounds a central black hole (see the review by Morris & Serabyn 1996). We conclude that while formation of nuclear clusters is an interesting problem, their existence does not offer any obvious insight into the formation of core versus power-law galaxies. This conclusion also applies to AGN, which in this sample offer little more than a ratification of the already standard notion that black holes are likely to exist at the centers of both types of galaxies.

The discovery of two more galaxies that have central minima in their brightness distributions in addition to the galaxies discussed in Lauer et al. (2002) implies that $\sim 5\%$ of core galaxies have such structures. As noted in Lauer et al. (2002), there are two competing ideas for the formation of these objects. In the first scenario, central minima might be explained by diffuse tori of stars added to a pre-existing core. The tori result from the tidal disruption of dense stellar aggregates transported to the center of the galaxy by dynamical friction following a merger; again, the black hole prevents the core once established from being filled in by latter mergers. In a second and more speculative scenario, the central minima are a direct consequence of stars ejected from the galaxy center by a binary black hole. It may be noteworthy that NGC 4073 and a number of the galaxies discussed in Lauer et al. (2002) have relatively high luminosities. In the discussion in that paper, we advanced the hypothesis that the mergers of two galaxies each with pre-existing cores, as would occur at the high-mass ends of a merging hierarchy, might be the necessary precondition for generating a merged galaxy in which the core was actually evacuated by the binary black hole. Under this picture, galaxies with central minima would be vivid examples of the action of binary black holes on central structure; however, present theoretical and observational treatment of this problem leaves this as an unproven hypothesis.

Likewise, we presently do not know what bearing galaxies with offset centers have on understanding the formation of central structure. If these systems are indeed unresolved analogs of the M31 nucleus, then their role may be more to show how nuclear black holes can stabilize non-axisymmetric structures in galaxy centers.

In Faber et al. (1997) we noted that power-law galaxies have disk-like outer isophotes; the conclusion here that all inclined power-law galaxies have visible stellar disks, with the implication that disks exist in *all* power-law galaxies, supports the dissipative formation scenario for power-law galaxies. Conversely, the corresponding lack of disks in all but the lowest-luminosity core galaxies supports their formation in dissipationless gas-free processes. A transition zone in galaxy luminosity where the dissipation and dissipationless stellar processes compete in mergers may explain the disks in the lower-luminosity galaxies with cores. Lastly, the rounder shapes of the inner isophotes of core galaxies as compared to power-law galaxies may be a direct consequence of core formation by a binary black hole on the presumption that scattering of stars by the binary is most likely to be nearly isotropic.

In the final analysis section, we have reasoned that the high prevalence of clumpy dust in non-equilibrium conditions means that it is generated in processes interior to the galaxies, themselves.

We have further argued that dust clouds once created settle into the center, and are eventual destroyed or processed by the galaxy on time scales of $\sim 10^8$ yr. The continued existence of dust clouds in a substantial fraction of early-type galaxies suggests that dust clouds are formed and destroyed in a cyclical process. The strong link between the presence of dust and nuclear emission argues that one outcome of this process would be episodic delivery of matter to the centers of the galaxies; understanding the secular evolution of cores may have to take this into account. At the same time we see no properties of present-day dust that bear one way or another on the basic formation mechanism of cores versus power-laws.

In conclusion, it appears that the diverse morphological measures derived for galaxies here give at most weak evidence for differences between core and power-law galaxies that might be taken as support for the binary black hole core formation mechanism. Dust is formed equally in both types, and the nuclei offer no apparent insight into this problem. Understanding the galaxies with central minima may offer a useful path for understanding core formation, but presently the mechanisms for forming central minima are too uncertain for forming conclusions. Position-angle twists, when properly normalized, seem equally strong in both types. Cores do have shallower color gradients, as expected, but the effect is weak. The strongest evidence comes from the rounder inner isophotes of cores and, more important, the high frequency of disks in the centers of power-law galaxies and (to a lesser degree) in the fainter core galaxies. Overall the evidence is consistent with the binary black hole core formation mechanism, but it is not a strong endorsement.

The real value of our data, we feel, is not in current tests of core formation, but in providing a rich set of observations that can be used to confront future models. Any successful model will have to match the large suite of quantitative data produced in this paper. Finally, we note that this paper does not consider the fundamental radial distribution of starlight in galaxies, which distinguishes cores from power-laws in the first place. This is the topic that taken up in Paper VI, where we demonstrate a strong dichotomy between the two types, validating the assumption of two classes in this paper.

This research was supported in part by several grants provided through STScI associated with GO programs 5512, 6099, 6587, 7388, 8591, 9106, and 9107. Our team meetings were generously hosted by the National Optical Astronomy Observatory, the Observatories of the Carnegie Institution of Washington, the Aspen Center for Physics, and the Leiden Observatory. We thank Dr. Barbara Ryden for useful conversations on isophote twists.

REFERENCES

- Bahcall, J. N., & Wolf, R. A. 1976, *ApJ*, 209, 214
- Begelman, M. C., Blandford, R. D., & Rees, M. J. 1980, *Nature*, 287, 307
- Bender, R., & Möllenhoff, C. 1987, *A&A*, 177, 71

- Bertola, F., Bettoni, D., Rusconi, L., & Sedmak, G. 1984, *AJ*, 89, 356
- Bertola, F., Buson, L. M., & Zeilinger, W. W. 1988, *Nature*, 335, 705
- Bertola, F., Cappellari, M., Funes, J. G., Corsini, E. M., Pizzella, A., & Vega Beltrán, J. C. 1998, *ApJ*, 509, L93
- Bertola, F., Cinzano, P., Corsini, E. M., Rix, H., & Zeilinger, W. W. 1995, *ApJ*, 448, L13
- Beuing, J., Bender, R., Mendes de Oliveira, C., Thomas, D., & Maraston, C. 2002, *A&A*, 395, 431
- Biller, B. A., Jones, C., Forman, W. R., Kraft, R., & Ensslin, T. 2004, *ApJ*, 613, 238
- Bower, G., et al. 2001, *ApJ*, 550, 75
- Buson, L. M., et al. 1993, *A&A*, 280, 409
- Byun, Y. I., et al. 1996, *AJ*, 111, 1889
- Caldwell, N. 1984, *PASP*, 96, 287
- Caon, N., Macchetto, D., & Pastoriza, M. 2000, *ApJS*, 127, 39
- Cappellari, M., Renzini, A., Greggio, L., di Serego Alighieri, S., Buson, L. M., Burstein, D., & Bertola, F. 1999, *ApJ*, 519, 117
- Carollo, C. M., Franx, M., Illingworth, G. D., & Forbes, D. 1997, *ApJ*, 481, 710
- Carter, D. L., Prieur, J. L., Wilkinson, A., Sparks, W. B., & Malin, D. F. 1988, *MNRAS*, 235, 813
- Chatterjee, P., Hernquist, L., & Loeb, A. 2002, *ApJ*, 572, 371
- Corsini, E. M., & Bertola, F. 1998, *Journal of Korean Physical Society*, 33, 574
- Crane, P., et al. 1993, *AJ*, 106, 1371
- de Koff, S. et al. 2000, *ApJS*, 129, 33
- Ebisuzaki, T., Makino, J., & Okumura, S. K. 1991, *Nature*, 354, 212
- Emsellem, E., et al. 2004, *MNRAS*, 352, 721
- Enßlin, T. A., & Heinz, S. 2002, *A&A*, 384, L27
- Fabbiano, G., Fassnacht, C., & Trinchieri, G. 1994, *ApJ*, 434, 67
- Faber, S. M., Tremaine, S., Ajhar, E. A., Byun, Y., Dressler, A., Gebhardt, K., Grillmair, C., Kormendy, J., Lauer, T. R., & Richstone, D. 1997, *AJ*, 114, 1771

- Faber, S. M., Wegner, G., Burstein, D., Davies, R. L., Dressler, A., Lynden-Bell, D., & Terlevich, R. J., 1989, *ApJS*, 69, 763
- Ferrarese, L., van den Bosch, F. C., Ford, H. C., Jaffe, W., & O’Connell, R. W. 1994, *AJ*, 108, 1598
- Ferrari, F., Pastoriza, M. G., Macchetto, F., & Caon, N. 1999, *A&AS*, 136, 269
- Fisher, D. 1997, *AJ*, 113, 950
- Fisher, D., Franx, M., & Illingworth, G. 1996, *ApJ*, 459, 110
- Fisher, D., Illingworth, G., & Franx, M. 1995, *ApJ*, 438, 539
- Forbes, D. A. 1991, *MNRAS*, 249, 779
- Fruchter, A. S., & Hook, R. N. 2002, *PASP*, 114, 144
- Gebhardt, K., Richstone, D., Ajhar, E. A., Lauer, T. R., Byun, Y., Kormendy, J., Dressler, A., Faber, S. M., Grillmair, C., & Tremaine, S. 1996, *AJ*, 112, 105
- Gebhardt, K., Richstone, D., Kormendy, J., Lauer, T. R., Ajhar, E. A., Bender, R., Dressler, A., Faber, S. M., Grillmair, C., Magorrian, J., & Tremaine, S. 2000, *AJ*, 119, 1157
- Gebhardt, K., et al. 2003, *ApJ*, 583, 92
- Gonzalez, J. G. 1993, Ph.D. Thesis, University of California, Santa Cruz
- Goudfrooij, P., & de Jong, T. 1995, *A&A*, 298, 784
- Goudfrooij, P., de Jong, T., Hansen, L., & Norgaard-Nielson, H. U. 1994a, *MNRAS*, 271, 833
- Goudfrooij, P., Hansen, L., Jorgensen, H. E., & Norgaard-Nielson, H. U. 1994a, *A&AS*, 105, 341
- Ho, L. C., Filippenko, A. V., & Sargent, W. L. W. 1995, *ApJS*, 98, 477.
- Ho, L. C., Filippenko, A. V., & Sargent, W. L. W. 1997, *ApJS*, 112, 315
- Holley-Bockelmann, K., & Richstone, D. O. 2000, *ApJ*, 531, 232
- Holtzman, J. A., Burrows, C. J., Casertano, S., Hester, J. J., Trauger, J. T., Watson, A. M., & Worthey, G. 1995, *PASP*, 107, 1065
- Humason, M. L., Mayall, N., & Sandage, A. R. 1956, *AJ*, 61, 97
- Jaffe, W., Ford, H., Ferrarese, L., van den Bosch, F., & O’Connell, R. W., 1996, *ApJ*, 460, 214
- Jaffe, W., Ford, H. C., O’Connell, R. W., van den Bosch, F. C., & Ferrarese, L. 1994, *AJ*, 108, 1567
- James, F., & Roos, M. 1977, CERN/D internal report 77/506

- Kannappan, S. J., & Fabricant, D. G. 2001, *AJ*, 121, 140
- Kim, D.-W. 1989, *ApJ*, 346, 653
- Knapp, G. R., Guhathakurta, P., Kim, D., & Jura, M. A. 1989, *ApJS*, 70, 329
- Kormendy, J. 1985, *ApJ*, 295, 73
- Kormendy, J., & Bender, R. 1996, *ApJ*, 464, L119
- Kormendy, J., Bender, R., Richstone, D., Ajhar, E. A., Dressler, A., Faber, S. M., Gebhardt, K., Grillmair, C., Lauer, T. R., & Tremaine, S. 1996, *ApJ*, 459, L57
- Kormendy, J., Dressler, A., Byun, Y.-I., Faber, S. M., Grillmair, C., Lauer, T. R., Richstone, D., & Tremaine, S. 1994, in *ESO/OHP Workshop on Dwarf Galaxies*, ed. G. Meylan & P. Prugniel (Garching: ESO), p. 147.
- Krist, J. 1995, *ASP Conf. Ser.* 77: *Astronomical Data Analysis Software and Systems IV*, 4, 349
- Laine, S., van der Marel, R. P., Lauer, T. R., Postman, M., O’Dea, C. P., & Owen, F. N. 2003, *AJ*, 125, 478
- Lauer, T. R. 1985, *ApJS*, 57, 473
- Lauer, T. R. 1986, *ApJ*, 311, 34
- Lauer, T. R. 1999a, *PASP*, 111, 227
- Lauer, T. R. 1999b, *PASP*, 111, 1434
- Lauer, T. R., Ajhar, E. A., Byun, Y.-I., Dressler, A., Faber, S. M., Grillmair, C., Kormendy, J., Richstone, D., & Tremaine, S. 1995, *AJ*, 110, 2622
- Lauer, T. R., Faber, S. M., Ajhar, E. A., Grillmair, C. J., & Scowen, P. A. 1998, *AJ*, 116, 2263
- Lauer, T. R., Tremaine, S., Ajhar, E. A., Bender, R., Dressler, A., Faber, S. M., Gebhardt, K., Grillmair, C., Kormendy, J., & Richstone, D. 1996, *ApJ*, 471, L79
- Lauer, T. R., et al. 1991, *ApJ*, 369, L41
- Lauer, T. R., et al. 1992a, *AJ*, 103, 703
- Lauer, T. R., et al. 1992b, *AJ*, 104, 552
- Lauer, T. R., et al. 1993, *AJ*, 106, 1436
- Lauer, T. R., et al. 2002, *AJ*, 124, 1975
- Laun, F., & Merritt, D. 2004, [astro-ph/0408029](https://arxiv.org/abs/astro-ph/0408029)

- Lucy, L. B. 1974, *AJ*, 79, 745
- Macchetto, F., Pastoriza, M., Caon, N., Sparks, W. B., Giavalisco, M., Bender, R., & Capaccioli, M. 1996, *A&AS*, 120, 463
- Magorrian, J., et al. 1998, *AJ*, 115, 2285
- Makino, J. 1997, *ApJ*, 478, 58
- Martel, A. R., Baum, S. A., Sparks, W. B., Wyckoff, E., Biretta, J. A., Golombek, D., Macchetto, F. D., de Koff, S., McCarthy, P. J., & Miley, G. K. 1999, *ApJS*, 122, 81
- Mathews, W. G., & Brighenti, F., 2003, *ApJ*, 590, L5
- McDermid, R., et al. 2004, *Astron. Nachr.*, 325, 100
- Michard, R. 1998, *A&A*, 335, 49
- Milosavljević, M., & Merritt, D. 2001, *ApJ*, 563, 34
- Möllenhoff, C., & Bender, R. 1987, *A&A*, 174, 63
- Morris, M., & Serabyn, E. 1996, *ARA&A*, 34, 645
- Nieto, J.-L., Macchetto, F. D., Perryman, M. A. C., di Serego Alighieri, S., & Lelievre, G. 1986, *A&A*, 165, 189
- Peiris, H., & Tremaine, S. 2003, *ApJ*, 599, 237
- Phillips, M. M., Jenkins, C. R., Dopita, M. A., Sadler, E. M., & Binette, L., 1986, *AJ*, 91, 1062
- Prugniel, P., & Simien, F. 1996, *A&A*, 309, 749
- Quinlan, G. D., & Hernquist, L. 1997, *New Astronomy*, 2, 533
- Raimond, E., Faber, S. M., Gallagher, J. S., & Knapp, G. R. 1981, *ApJ*, 246, 708
- Ravindranath, S., Ho, L. C., Peng, C. Y., Filippenko, A. V., & Sargent, W. L. W. 2001, *AJ*, 122, 653
- Rest, A., van den Bosch, F. C., Jaffe, W., Tran, H., Tsvetanov, Z., Ford, H. C., Davies, J., & Schafer, J. 2001, *AJ*, 121, 2431
- Richardson, W. H. 1972, *J. Opt. Soc. A.*, 62, 52
- Ryden, B. S., Forbes, D. A., & Terlevich, A. I. 2001, *MNRAS*, 326, 1141
- Ryden, B. S., Terndrup, D. M., Pogge, R. W., & Lauer, T. R. 1999, *ApJ*, 517, 650
- Sadler, E. M., & Gerhard, O. E. 1985, *MNRAS*, 214, 177

- Schweizer, F., & Seitzer, P. 1992, *AJ*, 104, 1039
- Shields, J. C., 1991, *AJ*, 102, 1314
- Sparks, W. B., Macchetto, F., & Golombek, D. 1989, *ApJ*, 345, 153
- Steiman-Cameron, T. Y., & Durisen, R. H. 1988, *ApJ*, 325, 26
- Tohline, J. E., Simonson, G. F., & Caldwell, N. 1982, *ApJ*, 252, 92
- Tomita, A., Aoki, K., Watanabe, M., Takata, T., & Ichikawa, S. 2000, *AJ*, 120, 123
- Tonry, J. L., Dressler, A., Blakeslee, J. P., Ajhar, E. A., Fletcher, A. B., Luppino, G. A., Metzger, M. R., & Moore, C. B. 2001, *ApJ*, 546, 681
- Tran, H. D., Tsvetanov, Z., Ford, H. C., Davies, J., Jaffe, W., van den Bosch, F. C., & Rest, A., 2001, *AJ*, 121, 2928
- Tremaine, S. 1995, *AJ*, 110, 628
- Tremaine, S., et al. 2002, *ApJ*, 574, 740
- van den Bosch, F. C., Ferrarese, L., Jaffe, W., Ford, H. C., & O’Connell, R.W. 1994, *AJ*, 108, 1579
- van den Bosch, F. C., & van der Marel, R. P. 1995, *MNRAS*, 274, 884
- van Dokkum, P. G., & Franx, M. 1995, *AJ*, 110, 2027
- van Gorkom, J. H., Knapp, G. R., Raimond, E., Faber, S. M., & Gallagher, J. S. 1986, *AJ*, 91, 79
- Verdoes Kleijn, G. A., Baum, S. A., de Zeeuw, P. T., & O’Dea, C. P., 1999, *AJ*, 118, 2592
- Verdoes Kleijn, G., & de Zeeuw, T. 2005, in preparation
- Véron-Cetty, M.-P., & Véron, P. 1988, *A&A*, 204, 28
- Vincent, R. A., & Ryden, B. S. 2005, in preparation
- Xilouris, E. M., Madden, S. C., Galliano, F., Vigroux, L., & Sauvage, M. 2004, *A&A*, 416, 41
- Yu, Q. 2002, *MNRAS*, 331, 935

Fig. 1.— *Available as standalone JPEG figures.* The deconvolved central $4'' \times 4''$ (88×88 PC1 pixels) regions of the galaxies are shown. The stretch is arbitrary and is adjusted to maximize image contrast over the portion of each galaxy shown. The image orientation is determined by how they were acquired in the PC1 CCD; arrows indicate the direction to north. Galaxies that were double-sampled (see §2.2) have been binned to the original pixel scale for this figure. For galaxies observed in multiple bandpasses, the F555W image has been shown. The panel to the right of each central image is the same region divided by a galaxy model reconstructed from the surface photometry; the contrast stretch is set to $\pm 50\%$ black to white. Galaxies with obscured centers are shown in Figure 2.

Fig. 2.— *Available as a standalone JPEG figure.* The central $4'' \times 4''$ (88×88 PC1 pixels) regions of the galaxies with dust-obscured centers are shown. These are objects for which no surface-brightness models could be derived. The image characteristics are otherwise the same as for Figure 1.

Fig. 3.— *Available as standalone GIF figures.* Surface photometry is shown for the unobscured galaxies. The top panel shows the surface brightness profile as a function of semi-major axis. Photometry is shown for the F555W filter, except for the few galaxies that were observed in this band. No Galactic absorption corrections have been applied. The solid line is a Nuker law (equation 1) fitted to the brightness profile; the extent of the line shows the radial range of the fit. The trace at the bottom of the panel shows the residuals from the Nuker law fit, referenced to the scale on the right side of the panel in magnitudes. The scale at the top of the panel is in parsecs, based on the distances given in Table 2. The next two thin panels for each galaxy give isophote position angle and ellipticity ($1 - \frac{b}{a}$). The range of the position angle plot varies depending on the range of isophote position angles observed; in some cases the minimum PA is negative to suppress abrupt 180° jumps. For the core galaxies, a dashed line shows fits of the PA as a function of radius to model described in §4.2. The bottom panel shows the $V - I$ profile with fitted gradient for those galaxies that have color information.

Table 1. Observational Summary

Galaxy	Program	Filter	Exposure (s)	Sky	Notes
NGC 0507	6587	F555W	2×800	22.44	
NGC 0584	6099	F814W	6×260	21.07	
		F555W	4×350	21.97	
NGC 0596	6587	F555W	4×400	22.36	Double-sampled
NGC 0741	6587	F555W	2×400	21.84	
NGC 0821	6099	F814W	6×260	21.28	Gebhardt et al. (2003)
		F555W	4×350	22.18	
NGC 1016	6587	F555W	2×800	22.37	
NGC 1023	6099	F814W	2×180	21.48	Bower et al. (2001)
		F555W	2×180	22.38	
	6587	F555W	5×260	21.40	Double-sampled
NGC 1316	5990	F814W	$600 + 260$	20.69	
NGC 1374	5446	F606W	2×80	22.57	
NGC 1399	8214	F606W	8×500	21.75	Double-sampled
NGC 1426	6587	F555W	4×400	22.22	Double-sampled
NGC 1427	5454	F814W	2×230	21.40	Carollo et al. (1997)
		F555W	2×500	22.50	
NGC 1439	5454	F814W	2×230	21.67	Carollo et al. (1997)
		F555W	2×500	22.57	
NGC 1700	5454	F814W	2×230	21.05	Carollo et al. (1997)
		F555W	2×500	21.95	
	6587	F555W	4×400	22.23	Double-sampled
NGC 2300	6099	F814W	6×230	21.56	
		F555W	4×350	22.46	
NGC 2434	5943	F450W	$1100 + 800$	23.21	
		F814W	$600 + 400$	21.54	
		F555W	$700 + 600$	22.26	
NGC 2768	6587	F555W	$4 \times 100 + 2 \times 500$	21.99	Double-sampled; obscured
NGC 2778	6099	F814W	6×260	21.73	Gebhardt et al. (2003)
		F555W	4×350	22.60	
NGC 2974	6587	F555W	$4 \times 100 + 2 \times 400$	22.94	Double-sampled
NGC 3115	5512	F814W	3×350	20.83	Kormendy et al. (1996)
		F555W	3×350	21.65	

Table 1—Continued

Galaxy	Program	Filter	Exposure (s)	Sky	Notes
NGC 3377	5512	F814W	3×350	21.38	Gebhardt et al. (2003)
		F555W	3×350	22.29	
NGC 3379	5512	F814W	3×400	21.40	Gebhardt et al. (2000)
		F555W	3×500	22.30	
NGC 3384	5512	F814W	3×350	22.35	Gebhardt et al. (2003)
		F555W	3×350	22.35	
NGC 3557	6587	F555W	2×900	...	Obscured
NGC 3585	6587	F555W	$4 \times 100 + 2 \times 400$	21.75	Double-sampled
NGC 3607	5999	F814W	$160 + 160$	21.24	
		F555W	160	22.21	
NGC 3608	5454	F814W	2×230	21.64	Carollo et al. (1997)
		F555W	2×500	22.54	
NGC 3610	6587	F555W	4×100	22.59	Double-sampled
NGC 3640	6587	F555W	$4 \times 100 + 2 \times 400$	21.82	Double-sampled
NGC 3706	6587	F555W	$4 \times 100 + 2 \times 500$	21.82	Double-sampled; Lauer et al. (2002)
NGC 3842	6587	F555W	2×800	22.54	
NGC 3945	6633	F450W	$1100 + 900$	22.36	
		F814W	$500 + 350$	21.77	
		F555W	$700 + 500$	22.68	
NGC 4026	9107	F814W	8×200	21.57	Double-sampled
		F555W	8×200	22.83	Double-sampled
NGC 4073	6587	F555W	2×800	22.30	
NGC 4125	6587	F555W	$4 \times 100 + 2 \times 500$...	Double-sampled; obscured
NGC 4278	5454	F814W	2×230	21.86	Carollo et al. (1997)
		F555W	2×500	22.76	
NGC 4291	6099	F814W	6×260	21.98	Gebhardt et al. (2003)
		F555W	4×350	22.88	
NGC 4365	5454	F814W	2×230	21.43	Carollo et al. (1997)
		F555W	2×500	22.33	
NGC 4382	7468	F814W	4×800	21.07	
		F555W	4×700	22.07	
NGC 4406	5512	F814W	3×500	21.40	Lauer et al. (2002)
		F555W	3×500	22.30	

Table 1—Continued

Galaxy	Program	Filter	Exposure (s)	Sky	Notes
NGC 4458	6587	F814W	2×800	21.55	
		F555W	$2 \times 400 + 199$	22.49	
NGC 4472	5236	F814W	2×900	21.40	
		F555W	2×900	22.30	
NGC 4473	6099	F814W	4×500	21.38	Gebhardt et al. (2003)
		F555W	3×600	22.32	
NGC 4478	6587	F555W	4×400	22.12	Double-sampled
NGC 4486B	6099	F814W	4×500	...	Lauer et al. (1996)
		F555W	3×600	...	
NGC 4494	5454	F814W	2×230	21.70	Carollo et al. (1997)
		F555W	2×500	22.60	
NGC 4552	6099	F814W	3×500	21.17	Carollo et al. (1997)
		F555W	4×600	22.15	
NGC 4589	5454	F814W	2×230	22.06	Carollo et al. (1997)
		F555W	2×500	22.96	
NGC 4621	5512	F814W	3×350	21.19	
		F555W	3×350	22.09	
NGC 4649	6286	F814W	$1300 + 1200$	21.40	Gebhardt et al. (2003)
		F555W	$1100 + 1000$	22.30	
NGC 4660	5512	F814W	4×200	20.89	
		F555W	4×230	21.85	
NGC 4709	6587	F555W	2×900	21.98	
NGC 4786	6587	F555W	4×100	...	Double-sampled; obscured
NGC 4936	6587	F555W	2×800	...	Obscured
NGC 5018	6587	F555W	4×100	21.94	Double-sampled; obscured
NGC 5061	6587	F555W	$4 \times 100 + 2 \times 400$	22.48	Double-sampled
NGC 5322	5454	F814W	2×230	...	Obscured; Carollo et al. (1997)
		F555W	2×500	...	
NGC 5419	6587	F555W	2×800	22.23	
NGC 5557	6587	F555W	$4 \times 100 + 2 \times 500$	22.78	Double-sampled
NGC 5576	9107	F814W	4×400	21.60	Double-sampled
		F555W	4×400	22.52	Double-sampled
NGC 5813	5454	F814W	2×230	21.51	Carollo et al. (1997)

Table 1—Continued

Galaxy	Program	Filter	Exposure (s)	Sky	Notes
		F555W	2×500	22.41	
NGC 5845	6099	F814W	4×260	...	Obscured
		F555W	3×400	...	
NGC 5982	5454	F814W	2×230	22.15	Carollo et al. (1997)
		F555W	2×500	23.15	
NGC 6776	6587	F555W	2×900	...	Obscured
NGC 6849	6587	F555W	2×900	22.56	
NGC 6876	6587	F814W	$2 \times 1400 + 1300$...	Lauer et al. (2002)
		F555W	$2 \times 1400 + 1300$...	
NGC 7213	9107	F814W	8×50	21.83	Double-sampled
		F555W	8×50	22.84	Double-sampled
NGC 7457	5512	F814W	3×350	21.93	Gebhardt et al. (2003)
		F555W	3×350	22.87	
NGC 7619	6554	F814W	$1300 + 900$	21.59	
		F555W	$1300 + 900$	22.49	
NGC 7626	5454	F814W	2×230	...	Obscured; Carollo et al. (1997)
		F555W	2×500	...	
NGC 7727	7468	F814W	4×800	20.61	
		F555W	$3 \times 700 + 533$	21.50	
NGC 7785	6587	F555W	$4 \times 100 + 2 \times 400$	22.43	Double-sampled
IC 1459	5454	F814W	2×230	21.59	Carollo et al. (1997)
		F555W	2×500	22.49	
IC 3370	6587	F555W	$4 \times 100 + 2 \times 500$...	Double-sampled; obscured
IC 4296	6587	F555W	2×800	...	Obscured
IC 4329	6587	F555W	2×800	22.56	
ESO 0462-015	6587	F555W	2×800	22.45	

Note. — “Double-sampled” refers to galaxies for which dithered images were used to construct an image with 2×2 pixel subsampling. “Obscured” means that the center of the galaxy was either not visible due to dust obscuration, or was so strongly affected by dust that accurate surface photometry could not be extracted. Sky values are in magnitudes per square arcsec. The references listed refer to earlier publication of surface photometry derived from the specific images listed.

Table 2. Global Parameters

Galaxy	Morph	D (Mpc)	Ref	M_V	σ (km/s)
NGC 0507	S0	63.8	4	–23.38	329
NGC 0584	E	22.1	1	–21.39	225
NGC 0596	E	22.1	1	–20.99	164
NGC 0741	E	70.9	4	–23.20	293
NGC 0821	E	25.5	1	–21.39	209
NGC 1016	E	75.9	3	–23.03	279
NGC 1023	S0	12.1	1	–20.51	212
NGC 1316	E	22.7	1	–23.34	250
NGC 1374	E	20.9	1	–20.75	207
NGC 1399	E	21.1	1	–22.07	359
NGC 1426	E	26.5	1	–20.80	153
NGC 1427	E	21.0	1	–20.78	170
NGC 1439	E	26.5	1	–20.98	159
NGC 1700	E	40.6	2	–21.94	234
NGC 2300	S0	30.4	4	–21.72	252
NGC 2434	E	22.8	1	–22.01	229
NGC 2768	E	23.3	1	–21.90	194
NGC 2778	E	24.2	1	–19.52	166
NGC 2974	E	22.7	1	–21.33	143
NGC 3115	S0-	10.2	1	–21.17	271
NGC 3377	E	11.7	1	–20.04	143
NGC 3379	E	11.7	1	–20.90	221
NGC 3384	S0-	11.7	1	–19.88	158
NGC 3557	E	48.3	1	–23.23	265
NGC 3585	E	21.2	1	–22.01	216
NGC 3607	E	10.9	1	–20.64	220
NGC 3608	E	23.0	1	–21.11	195
NGC 3610	E	22.6	1	–20.88	167
NGC 3640	E	28.3	1	–21.97	184
NGC 3706	S0-	46.9	4	–22.49	302
NGC 3842	E (BGC)	97.0	1	–23.22	316
NGC 3945	S0	19.9	3	–21.14	176
NGC 4026	S0	15.6	1	–20.32	193

Table 2—Continued

Galaxy	Morph	D (Mpc)	Ref	M_V	σ (km/s)
NGC 4073	E	92.2	4	−23.62	266
NGC 4125	E	25.2	1	−22.34	233
NGC 4278	E	16.7	1	−21.05	251
NGC 4291	E	25.0	1	−20.56	284
NGC 4365	E	21.6	1	−22.02	269
NGC 4382	S0	17.9	1	−22.28	184
NGC 4406	E	17.9	1	−22.28	246
NGC 4458	E	17.9	1	−19.32	101
NGC 4472	E	17.9	1	−22.92	303
NGC 4473	E	17.9	1	−20.99	179
NGC 4478	E	17.9	1	−19.98	144
NGC 4486B	cE	17.9	1	−17.91	178
NGC 4494	E	17.9	1	−21.48	155
NGC 4552	E	17.9	1	−21.39	263
NGC 4589	E	25.0	1	−21.33	225
NGC 4621	E	17.9	1	−21.61	237
NGC 4649	E	17.9	1	−22.49	343
NGC 4660	E	17.9	1	−20.09	191
NGC 4709	E	37.0	1	−22.31	239
NGC 4786	E+p	70.7	4	−22.58	295
NGC 4936	E	50.1	4	−23.26	278
NGC 5018	E	42.6	3	−22.61	212
NGC 5061	E	26.9	4	−21.94	194
NGC 5322	E	33.0	1	−22.40	234
NGC 5419	E	62.6	4	−23.43	315
NGC 5557	E	52.7	4	−22.61	253
NGC 5576	E	27.1	1	−21.67	188
NGC 5813	E	28.7	1	−21.84	230
NGC 5845	E	28.7	1	−19.84	241
NGC 5982	E	40.5	4	−22.01	250
NGC 6776	E+p	77.6	4	−22.80	209
NGC 6849	S0-	84.0	4	−23.32	207
NGC 6876	E	57.6	4	−23.74	230

Table 2—Continued

Galaxy	Morph	D (Mpc)	Ref	M_V	σ (km/s)
NGC 7213	Sa	22.7	3	−21.51	185
NGC 7457	S0-	14.0	1	−18.63	78
NGC 7619	E	56.1	1	−22.93	319
NGC 7626	E	56.0	1	−22.49	269
NGC 7727	Sa	21.6	3	−21.33	200
NGC 7785	E	49.9	4	−22.14	253
IC 1459	E	30.9	1	−22.56	311
IC 3370	E	28.3	1	−21.55	202
IC 4296	E (BCG)	45.4	2	−23.32	340
IC 4329	E (BCG)	56.7	2	−23.70	270
ESO 462-15	E	80.3	4	−22.88	289

Note. — Morphological classifications are from the NASA/IPAC Extragalactic Database; BGC means that the galaxy is a brightest cluster galaxy. Distance reference codes: (1) Tonry et al. (2001) SBF distances scaled to $H_0 = 70 \text{ km s}^{-1} \text{ Mpc}^{-1}$; (2) distance from Faber et al. (1997) scaled to $H_0 = 70$; (3) Faber et al. (1989) group distance scaled to $H_0 = 70$; and (4) distance based on CMB velocity of galaxy or group. Velocity dispersions are provided by the Prugniel & Simien (1996) compendium of all published velocity dispersions.

Table 3. Central Properties

Galaxy	Dust			Stellar		Pec	Spec Type	Emiss Class	Ref
	Str	Morph	Conc	Disk	Nuc				
NGC 0507	0.0					Offset	a	0	1,3,8
NGC 0584	0.5	c	2				E:	1:	3,5,6,8,12
NGC 0596	0.0				×		a	0	4,5,8,9,12
NGC 0741	0.0	nr	2		×		E	1	5,13
NGC 0821	0.0			×			a	0	1,3,4,5,8
NGC 1016	0.1								
NGC 1023	0.0			×	×		a	0	1
NGC 1316	4.1	c	1		×		E	2	2,12
NGC 1374	0.3					Offset	a	0	2
NGC 1399	0.0				×		a	0.5	2,4,8,12
NGC 1426	0.0				×		E	1	9
NGC 1427	0.0			×	×		a	0	2
NGC 1439	2.4	nr	2		×		a	0	14
NGC 1700	0.2	c	2				E	1	3,4,9
NGC 2300	0.0						a	0	1,3,4
NGC 2434	3.0	nr	2		×		a:	0:	2,12
NGC 2768	...	s	1				L2	2	1,7,9
NGC 2778	0.3	nr:	2		×		E:	2:	3
NGC 2974	2.5	s	1				E	2	4,6,7,8,11,12
NGC 3115	0.1			×	×		a	0	1,5
NGC 3377	0.0	c	1	×			a	0.5	1,3,4,9
NGC 3379	1.9	nr	2				L2/T2::	1	1,3,4,5
NGC 3384	0.0			×	×		a	0	1
NGC 3557	...	nr	2				E	2	2,4,8,9
NGC 3585	1.6	nr	2	×			a	0	6,8
NGC 3607	8.7	t	1				L 2	2	1,5,6
NGC 3608	0.2	nr:	2				L2/S2:	1	1,3,4
NGC 3610	0.0			×			a	0	1,4,9
NGC 3640	0.2						a	0	1,4
NGC 3706	0.0			×		Bar	a	0	4,10
NGC 3842	0.0								
NGC 3945	1.2	c	1		×		L2	2	1

Table 3—Continued

Galaxy	Dust			Stellar Disk	Nuc	Pec	Spec Type	Emiss Class	Ref
	Str	Morph	Conc						
NGC 4026	0.0	c	1	×	×		a	0	1
NGC 4073	0.0					Min	a	0	14
NGC 4125	...	c	1				T2	2	1,4,7
NGC 4278	3.8	s	1		×		L2	3	1,3,4
NGC 4291	0.0					Offset:	a	0	1
NGC 4365	0.0				×		a	0	1,4,6,8
NGC 4382	0.0					Min	a	0	1,6,8
NGC 4406	0.0				×	Min	a	0	1,6,8
NGC 4458	0.2			×					
NGC 4472	0.7	c	2		×		S2::	1	1,3,5,6
NGC 4473	0.0			×			a	0	1,4,5,6
NGC 4478	0.0			×	×		a	0	1,3
NGC 4486B	0.0					Min			
NGC 4494	5.3	nr	2				L2::	1	1
NGC 4552	0.5	c	1		×		T2:	1.5	1,3,5,6,9
NGC 4589	6.7	c	1				L2	2	1,4,7
NGC 4621	0.0			×			a	0	1,4,6,8
NGC 4649	0.0						a	0	1,3,6,7,8
NGC 4660	0.0			×			a	0	1,4
NGC 4709	0.0				×				
NGC 4786	...	nr	2				E	1	9
NGC 4936	...	c	1				E	2	5,10
NGC 5018	...	t	1				E:	1:	4,7,8,9,10
NGC 5061	0.0						a	0	4,8
NGC 5322	...	nr	2				L2::	1	1,4,7,9
NGC 5419	0.1				×	double?	E:	1:	2,5,12
NGC 5557	0.1						a	0	1,9
NGC 5576	0.0					Offset:	a	0	1,4,9
NGC 5813	0.5	t	1				L2:	1	1,3,4,5,8
NGC 5845	...	nr	2						
NGC 5982	0.1						L2::	1	1,9
NGC 6776	...	t					E	2	2,5,9,10

Table 3—Continued

Galaxy	Dust			Stellar			Spec Type	Emiss Class	Ref
	Str	Morph	Conc	Disk	Nuc	Pec			
NGC 6849	0.0						a	0	2,10
NGC 6876	0.0	c	0			Min	E	1	2,5,6
NGC 7213	4.0	s	1		×		S1	2	2,8
NGC 7457	0.0				×		c+a	0	1
NGC 7619	0.0					Offset	a	0	1,3,5,6
NGC 7626	...	nr	2				L2::	1	1,3,5,6,13
NGC 7727	6.2	s	1				E	2	8
NGC 7785	2.7	c	2				E	1	3,9
IC 1459	3.7	t	1		×		E	3	4,5,6,9,11
IC 3370	...	s	1				E	2	4,8
IC 4296	...	nr	2				E	1	2,5,6,9
IC 4329	0.2						a	0	10
ESO 0462-015	0.1				×				

Note. — Colons indicate weak and/or uncertain quantities. Numbers under dust strength are hundredths of magnitudes of dust absorption within 1'' of the galaxy centers; “...” indicates dusty galaxies for which a Nuker law model could not be constructed; the value for NGC 7457 was set to 0.0 by inspection. Dust morphologies: nr = well defined nuclear dust ring or disk, c = chaotic, disorganized dust patches, s = spiral dust lanes, t = transition case between nuclear ring and non-ring (i.e., between nr and c/s). Dust concentration classes: 0 = dust present only outside 4'' postage stamp in Figure 1, 1 = dust present both within 4'' postage stamp and outside it, 2 = virtually all dust inside 4'' postage stamp. A “×” in the stellar disk column indicates galaxies with stellar disks visible into their centers in the subtracted-model postage stamps in Figure 1. The nucleus column indicates that a nucleus is detected using the method explained in the text. Peculiarities: “Min” indicates a brightness depression in the central pixel(s); “Offset” indicates that the central stellar peak is offset from the outer isophotes; “Bar” indicates a bright central bar (or edge-on disk). Spectral types are taken preferentially from Ho et al. (1997), otherwise from the literature. An “a” indicates an absorption spectrum with no (or very small) emission, “L” means a LINER nucleus, “T” a LINER/H II transition object, “S” a Seyfert nucleus, and “E” indicates general emission of an unclassified type. The “c+a” for NGC 7457 indicates

a suspected nuclear continuum source plus absorption. The numbers “1” and “2” under spectral type signify broad and narrow permitted lines, respectively. Emission-strength class: 0 = no emission detected, 1 = weak emission, 2 = strong emission, 3 = very strong emission. Emission classes were determined by intercomparison of data from the references in the last column. Emission references: 1 = Ho et al. (1997); 2 = Phillips et al. (1986); 3 = Gonzalez (1993); 4 = Goudfrooij et al. (1994a); 5 = Macchetto et al. (1996); 6 = Shields (1991); 7 = Kim (1989); 8 = Véron-Cetty & Véron (1988); 9 = Caldwell (1984); 10 = Carter et al. (1988); 11 = Buson et al. (1993); 12 = Beuing et al. (2002); 13 = Verdoes Kleijn et al. (1999); 14 = Humason et al. (1956).

Table 4. Central Structural Parameters

Galaxy	P	r_b (pc)	θ_b	$I_b(V)$	α	β	γ	γ'	Notes
NGC 0507	\cap	343.3	1.11	17.16	1.26	1.75	0.00	0.01	
NGC 0584	\cap	47.1	0.44	15.22	0.47	1.61	-0.01	0.30	
NGC 0596	\setminus	4.3	0.54	15.90	0.45	1.59	0.16	0.54	
NGC 0741	\cap	391.9	1.14	17.67	2.27	1.29	0.10	0.11	
NGC 0821	\wedge	59.3	0.48	15.69	0.43	1.71	0.10	0.42	\setminus in Rav.
NGC 1016	\cap	618.2	1.68	18.01	0.98	1.90	0.09	0.11	
NGC 1023	\setminus	2.3	1.23	15.71	7.23	1.15	0.74	0.74	
NGC 1316	\cap	41.8	0.38	14.41	1.01	1.23	-0.10	0.13	$V - I = 1.40$
NGC 1374	\cap	9.1	0.09	14.57	1.87	1.08	-0.09	-0.03	$V - R = 0.60$
NGC 1399	\cap	324.3	3.17	17.23	1.58	1.63	0.09	0.09	$V - R = 0.60$
NGC 1426	\setminus	5.1	1.25	16.98	0.51	1.80	0.25	0.56	
NGC 1427	\setminus	4.1	0.86	16.25	0.79	1.67	0.30	0.51	
NGC 1439	\setminus	5.1	0.65	16.21	4.82	1.48	0.74	0.74	
NGC 1700	\cap	11.8	0.06	13.58	1.03	1.19	-0.10	0.07	\setminus in L95
NGC 2300	\cap	330.1	2.24	17.53	1.20	1.80	0.07	0.08	
NGC 2434	\setminus	4.4	5.41	19.10	1.95	2.05	0.75	0.75	
NGC 2778	\setminus	4.7	0.35	16.06	0.41	1.75	0.33	0.83	
NGC 2974	\setminus	4.4	0.44	15.41	15.72	1.10	0.62	0.62	
NGC 3115	\setminus	2.0	0.86	14.48	4.30	1.09	0.52	0.52	
NGC 3377	\setminus	2.3	0.31	14.12	0.30	1.96	0.03	0.62	
NGC 3379	\cap	112.3	1.98	16.15	1.54	1.54	0.18	0.18	
NGC 3384	\setminus	2.3	3.15	16.44	15.32	1.81	0.71	0.71	
NGC 3585	\wedge	37.0	0.36	14.72	1.62	1.06	0.31	0.31	
NGC 3607	\cap	128.4	2.43	16.87	2.06	1.70	0.26	0.26	
NGC 3608	\cap	53.5	0.48	15.73	0.92	1.50	0.09	0.17	
NGC 3610	\setminus	4.4	2.84	16.39	48.48	1.86	0.76	0.76	
NGC 3640	\cap	46.6	0.34	15.66	0.64	1.30	-0.10	0.03	\wedge in Rest
NGC 3706	\cap	40.9	0.18	14.18	14.66	1.24	-0.01	-0.01	
NGC 3842	\cap	507.9	1.08	17.76	1.84	1.42	0.15	0.15	
NGC 3945	\setminus	3.9	7.38	18.62	0.30	2.56	-0.06	0.57	
NGC 4026	\setminus	3.0	0.63	15.23	0.39	1.78	0.15	0.65	
NGC 4073	\cap	129.6	0.29	16.53	4.43	0.99	-0.08	-0.08	
NGC 4278	\cap	102.0	1.26	16.20	1.40	1.46	0.06	0.10	

Table 4—Continued

Galaxy	P	r_b (pc)	θ_b	$I_b(V)$	α	β	γ	γ'	Notes
NGC 4291	∩	72.7	0.60	15.66	1.52	1.60	0.01	0.02	
NGC 4365	∩	231.4	2.21	16.88	1.74	1.52	0.07	0.09	
NGC 4382	∩	80.7	0.93	15.67	1.13	1.39	0.00	0.01	
NGC 4406	∩	79.8	0.92	16.03	3.87	1.04	−0.04	−0.04	
NGC 4458	∩	7.8	0.09	13.72	4.55	1.40	0.16	0.17	\ in L95
NGC 4472	∩	211.7	2.44	16.63	1.89	1.17	0.01	0.01	
NGC 4473	∩	386.2	4.45	17.24	0.66	2.60	−0.07	0.01	
NGC 4478	∩	19.1	0.22	15.46	1.88	1.01	−0.10	0.10	\ in L95
NGC 4486B	∩	13.9	0.16	14.53	2.82	1.39	−0.10	−0.10	
NGC 4494	\	3.5	2.82	17.19	0.68	1.88	0.52	0.55	
NGC 4552	∩	42.5	0.49	15.20	1.97	1.17	−0.10	−0.02	
NGC 4589	∩	67.9	0.56	16.08	1.05	1.32	0.21	0.25	
NGC 4621	\	3.5	1.00	15.76	0.41	1.34	0.75	0.85	
NGC 4649	∩	437.4	5.04	17.28	1.67	1.58	0.16	0.16	
NGC 4660	\	3.5	1.76	16.34	5.61	1.50	0.91	0.91	
NGC 4709	∩	222.4	1.24	17.46	1.89	1.47	0.27	0.28	
NGC 5061	∩	37.8	0.29	14.35	1.64	1.43	0.04	0.05	
NGC 5419	∩	722.3	2.38	17.87	1.43	1.69	−0.10	0.03	
NGC 5557	∩	204.4	0.80	16.40	0.80	1.68	0.02	0.07	∧ in Rest
NGC 5576	∩	549.2	4.18	17.81	0.43	2.73	0.01	0.26	\ in Rest
NGC 5813	∩	162.0	1.17	16.86	1.06	1.81	−0.10	−0.08	
NGC 5982	∩	68.7	0.35	15.66	2.07	1.03	0.05	0.05	
NGC 6849	∩	138.5	0.34	17.03	1.01	1.21	0.01	0.08	
NGC 6876	∩	139.6	0.50	16.99	12.07	0.75	0.00	0.00	
NGC 7213	∩	383.0	3.48	17.71	1.03	3.10	0.06	0.21	
NGC 7457	\	2.7	0.22	16.33	1.01	1.05	−0.10	0.61	∧ in Rav.
NGC 7619	∩	220.3	0.81	16.40	1.08	1.62	−0.02	0.01	
NGC 7727	∧	601.1	5.74	18.42	0.57	1.93	0.43	0.49	
NGC 7785	∩	14.5	0.06	15.09	0.95	0.92	−0.10	0.05	
IC 1459	∩	293.6	1.96	16.36	0.80	2.08	−0.10	0.15	
IC 4329	∩	261.2	0.79	16.37	2.87	1.31	0.01	0.01	
ESO 462-015	\	15.6	0.41	16.59	0.20	1.77	−0.10	0.56	

Note. — The profile type, P, is \backslash = power-law, \wedge = intermediate form, and \cap = core. θ_b is the angular break radius in arcseconds along the major axis. The Nuker law parameters are defined in equation (1). The surface brightness, I_b , is in units of V mags per square arcsec. No Galactic absorption corrections have been applied, but NGC 1316, 1374, and 1399 have been transformed to the V band using the color terms in the notes column. γ' is the power-law slope $-d \log I / d \log r$ at the inner resolution limit, which is $0''.02$ for dithered images, or $0''.04$ otherwise. The notes column lists references with differing profile classifications, where L95=Lauer et al. (1995), Rest=Rest et al. (2001), and Rav.=Ravindranath et al. (2001).

Table 5. Average Ellipticity

Galaxy	P	Inner Ellipticity	Outer Ellipticity
NGC 507	\cap	0.229	0.190
NGC 584	\cap	0.346	0.255
NGC 596	\setminus	0.123	0.072
NGC 741	\cap	0.043	0.147
NGC 821	\wedge	0.370	0.382
NGC 1016	\cap	0.099	0.071
NGC 1023	\setminus	0.351	0.201
NGC 1316	\cap	0.242	0.367
NGC 1374	\cap	0.036	0.110
NGC 1399	\cap	0.078	0.125
NGC 1426	\setminus	0.320	0.315
NGC 1427	\setminus	0.287	0.293
NGC 1439	\setminus	0.274	0.148
NGC 1700	\cap	0.318	0.294
NGC 2300	\cap	0.196	0.232
NGC 2434	\setminus	0.083	0.067
NGC 2778	\setminus	0.111	0.204
NGC 2974	\setminus	0.296	0.301
NGC 3115	\setminus	0.537	0.548
NGC 3377	\setminus	0.360	0.509
NGC 3379	\cap	0.102	0.097
NGC 3384	\setminus	0.415	0.180
NGC 3585	\wedge	0.283	0.456
NGC 3607	\cap	0.129	0.159
NGC 3608	\cap	0.108	0.184
NGC 3610	\setminus	0.437	0.516
NGC 3640	\cap	0.110	0.212
NGC 3842	\cap	0.044	0.174
NGC 3945	\setminus	0.191	0.299
NGC 4026	\setminus	0.469	0.385
NGC 4278	\cap	0.155	0.167
NGC 4291	\cap	0.260	0.247

Table 5—Continued

Galaxy	P	Inner Ellipticity	Outer Ellipticity
NGC 4365	∩	0.286	0.248
NGC 4382	∩	0.262	0.240
NGC 4458	∩	0.573	0.187
NGC 4472	∩	0.088	0.110
NGC 4473	∩	0.469	0.412
NGC 4478	∩	0.311	0.220
NGC 4486	∩	0.431	0.124
NGC 4494	\	0.225	0.153
NGC 4552	∩	0.138	0.050
NGC 4589	∩	0.399	0.197
NGC 4621	\	0.299	0.351
NGC 4649	∩	0.072	0.140
NGC 4660	\	0.396	0.404
NGC 4709	∩	0.233	0.184
NGC 5061	∩	0.060	0.038
NGC 5419	∩	0.180	0.208
NGC 5557	∩	0.089	0.209
NGC 5576	∩	0.242	0.302
NGC 5813	∩	0.124	0.107
NGC 5982	∩	0.031	0.273
NGC 6849	∩	0.056	0.353
NGC 7213	∩	0.108	0.110
NGC 7457	\	0.064	0.371
NGC 7619	∩	0.392	0.266
NGC 7727	∧	0.262	0.243
NGC 7785	∩	0.266	0.367
IC 1459	∩	0.260	0.261
IC 4329	∩	0.168	0.152
ESO 462-15	\	0.170	0.271

Note. — uminosity-weighted average isophote ellipticity for $r \leq r_b$ and $r > r_b$. Parameters were not measured for NGC 4073, 4406, 4486B, and 6876, which have central surface brightness minima.

Table 6. Nuclei Luminosities and Colors

Galaxy	P	m_V	$V - I$	$\Delta(V - I)$	M_V	$L/L_\odot(V)$
NGC 0596	\	21.8	-10.0	9×10^5
NGC 0741	∩	21.9	-12.5	9×10^6
NGC 1023	\	19.5	0.9	-0.4	-11.1	3×10^6
NGC 1316	∩	19.9	-12.0	5×10^6
NGC 1399	∩	24.4	-7.2	7×10^4
NGC 1426	\	19.6	-12.5	9×10^6
NGC 1427	\	19.6	1.3	0.0	-12.0	6×10^6
NGC 1439	\	20.2	1.1	-0.2	-11.9	5×10^6
NGC 2434	\	20.3	0.7	-0.5	-12.3	7×10^6
NGC 2778	\	20.0	1.3	-0.1	-11.9	5×10^6
NGC 3115	\	17.8	1.2	-0.1	-12.3	8×10^6
NGC 3384	\	18.9	1.3	0.0	-11.5	4×10^6
NGC 3945	\	20.9	1.5	0.2	-10.7	2×10^6
NGC 4026	\	19.5	1.3	0.0	-11.6	4×10^6
NGC 4278	∩	19.5	0.4	-0.8	-11.7	4×10^6
NGC 4365	∩	21.0	0.6	-0.7	-10.6	2×10^6
NGC 4406	∩	22.9	1.2	0.0	-8.4	2×10^5
NGC 4472	∩	22.7	1.0	-0.4	-8.6	2×10^5
NGC 4478	∩	19.7	-11.6	4×10^6
NGC 4552	∩	20.5	1.3	0.0	-10.9	2×10^6
NGC 4709	∩	23.2	-10.0	8×10^5
NGC 5419	∩	19.8	-14.4	5×10^7
NGC 7213	∩	16.6	0.6	-0.8	-15.2	1×10^8
NGC 7457	\	18.1	1.2	0.1	-12.7	1×10^7
IC 1459	∩	18.4	1.0	-0.4	-14.0	4×10^7

Note. — All photometry has been corrected for Galactic extinction $\Delta(V - I)$ gives the color of the nucleus relative to the host galaxy immediately outside the nucleus. M_V is the nuclear absolute magnitude estimated by subtracting off the Nuker law fit to the pixels beyond the nucleus. The last column gives the V band nuclear luminosity in solar units.

Table 7. Central Color Gradients

Galaxy	$V - I$	$d(V - I)/d \log(r)$
NGC 0584	1.266 ± 0.003	-0.084 ± 0.007
NGC 0821	1.350 ± 0.001	-0.056 ± 0.002
NGC 1023	1.258 ± 0.002	-0.039 ± 0.004
NGC 1427	1.237 ± 0.002	-0.066 ± 0.004
NGC 1439	1.274 ± 0.004	-0.125 ± 0.008
NGC 1700	1.289 ± 0.002	-0.051 ± 0.003
NGC 2300	1.329 ± 0.001	$+0.005 \pm 0.002$
NGC 2434	1.231 ± 0.004	-0.092 ± 0.008
NGC 2778	1.280 ± 0.002	-0.053 ± 0.004
NGC 3115	1.278 ± 0.002	-0.046 ± 0.005
NGC 3377	1.229 ± 0.003	-0.028 ± 0.006
NGC 3379	1.282 ± 0.001	-0.029 ± 0.003
NGC 3384	1.252 ± 0.002	-0.047 ± 0.004
NGC 3607	1.360 ± 0.013	-0.058 ± 0.026
NGC 3608	1.289 ± 0.002	-0.068 ± 0.004
NGC 3945	1.278 ± 0.002	-0.063 ± 0.003
NGC 4026	1.258 ± 0.003	-0.041 ± 0.005
NGC 4278	1.264 ± 0.003	-0.028 ± 0.006
NGC 4291	1.271 ± 0.001	-0.036 ± 0.003
NGC 4365	1.325 ± 0.002	-0.034 ± 0.004
NGC 4382	1.108 ± 0.001	$+0.006 \pm 0.003$
NGC 4406	1.253 ± 0.003	-0.028 ± 0.006
NGC 4458	1.176 ± 0.002	-0.010 ± 0.004
NGC 4472	1.330 ± 0.002	-0.027 ± 0.004
NGC 4473	1.280 ± 0.001	-0.039 ± 0.002
NGC 4486B	1.247 ± 0.002	-0.016 ± 0.003
NGC 4494	1.257 ± 0.006	-0.137 ± 0.013
NGC 4552	1.289 ± 0.001	-0.027 ± 0.002
NGC 4589	1.331 ± 0.004	-0.142 ± 0.010
NGC 4621	1.300 ± 0.003	-0.018 ± 0.005
NGC 4649	1.338 ± 0.001	-0.008 ± 0.002
NGC 4660	1.296 ± 0.001	-0.051 ± 0.003
NGC 5576	1.183 ± 0.001	-0.022 ± 0.003

Table 7—Continued

Galaxy	$V - I$	$d(V - I)/d \log(r)$
NGC 5813	1.310 ± 0.013	$+0.018 \pm 0.026$
NGC 5982	1.264 ± 0.003	-0.033 ± 0.006
NGC 7213	1.440 ± 0.028	$+0.127 \pm 0.057$
NGC 7457	1.122 ± 0.009	$+0.027 \pm 0.019$
NGC 7619	1.353 ± 0.002	-0.059 ± 0.005
NGC 7727	0.570 ± 0.007	-0.122 ± 0.015
IC 1459	1.369 ± 0.004	-0.087 ± 0.008

Note. — $V - I$ colors are given at $1''$ from the galaxy centers. Colors have been corrected for Galactic extinction.

Table 8. Isophote PA Gradients and Twists

Galaxy	Twist Radius (arcsec)	γ'	Inner	Outer	Inner Twist	Outer Twist
			Gradient $\frac{\Delta\text{PA(deg)}}{\Delta\log(r)}$	Gradient $\frac{\Delta\text{PA(deg)}}{\Delta\log(r)}$		
NGC 0507	0.50	0.47	-64.2	4.2	1.1×10^{-2}	1.0×10^{-2}
NGC 0584	0.67	0.87	-4.1	2.1	6.4×10^{-3}	4.6×10^{-3}
NGC 0596	3.82	1.17	-0.6	-92.5	1.0×10^{-2}	1.4×10^{-2}
NGC 0741	1.08	0.67	116.5	-4.9	8.3×10^{-3}	3.2×10^{-3}
NGC 0821	0.78	0.99	3.9	0.1	4.0×10^{-3}	1.3×10^{-3}
NGC 1016	0.46	0.48	-70.3	-1.5	8.2×10^{-3}	1.9×10^{-3}
NGC 1023	1.44	1.05	1.0	5.0	7.0×10^{-3}	2.7×10^{-3}
NGC 1316	1.08	0.89	40.0	-6.0	2.7×10^{-2}	1.3×10^{-2}
NGC 1374	0.32	0.98	10.5	0.1	2.1×10^{-3}	1.1×10^{-3}
NGC 1399	0.48	0.16	7.4	1.8	3.9×10^{-3}	2.7×10^{-3}
NGC 1426	0.30	0.75	5.2	3.4	1.3×10^{-2}	7.9×10^{-3}
NGC 1427	0.55	0.86	8.6	-0.4	5.1×10^{-3}	2.6×10^{-3}
NGC 1439	0.78	1.27	-0.9	-15.7	3.8×10^{-2}	1.8×10^{-2}
NGC 1700	0.30	0.98	6.0	-1.3	8.4×10^{-3}	1.0×10^{-2}
NGC 2300	0.57	0.34	46.6	-4.7	3.8×10^{-3}	3.3×10^{-3}
NGC 2434	0.50	0.76	-113.2	22.9	2.1×10^{-2}	5.0×10^{-3}
NGC 2778	4.68	1.39	6.0	-11.7
NGC 2974	0.39	0.68	-15.7	-2.3	2.7×10^{-2}	4.7×10^{-2}
NGC 3115	0.78	0.75	1.0	0.0	3.4×10^{-2}	4.6×10^{-3}
NGC 3377	1.76	1.24	0.4	0.0	2.2×10^{-3}	3.0×10^{-3}
NGC 3379	0.67	0.39	-50.0	7.4	5.9×10^{-3}	2.9×10^{-3}
NGC 3384	4.68	1.81	0.6	19.4
NGC 3585	0.43	0.74	-14.6	-0.6	7.3×10^{-3}	3.5×10^{-3}
NGC 3607	1.08	0.49	-87.8	58.2	2.1×10^{-2}	4.6×10^{-2}
NGC 3608	0.57	0.85	34.1	1.0	6.9×10^{-3}	7.2×10^{-4}
NGC 3610	1.04	0.76	9.5	-6.6	1.3×10^{-2}	1.0×10^{-2}
NGC 3640	0.34	0.60	15.8	-11.9	6.6×10^{-3}	6.2×10^{-3}
NGC 3842	0.78	0.60	-148.0	18.8	8.0×10^{-3}	2.6×10^{-3}
NGC 3945	2.87	1.07	-23.8	57.1	2.7×10^{-2}	6.2×10^{-2}
NGC 4026	0.30	0.84	-2.3	1.2	8.9×10^{-3}	1.6×10^{-2}
NGC 4278	0.46	0.33	61.1	4.7	1.0×10^{-2}	6.4×10^{-3}

Table 8—Continued

Galaxy	Twist Radius (arcsec)	γ'	Inner Gradient $\frac{\Delta\text{PA}(\text{deg})}{\Delta\log(r)}$	Outer Gradient $\frac{\Delta\text{PA}(\text{deg})}{\Delta\log(r)}$	Inner Twist	Outer Twist
NGC 4291	3.38	1.50	0.8	−2.0	1.6×10^{-3}	2.7×10^{-3}
NGC 4365	1.76	0.65	−3.4	0.6	1.0×10^{-3}	1.3×10^{-3}
NGC 4382	1.50	0.88	−16.4	0.0	6.5×10^{-3}	5.0×10^{-3}
NGC 4458	1.50	1.40	0.0	0.7	2.9×10^{-3}	7.4×10^{-4}
NGC 4472	0.67	0.10	−56.3	−12.3	3.7×10^{-3}	2.0×10^{-3}
NGC 4473	0.46	0.42	6.4	0.2	2.6×10^{-3}	1.1×10^{-3}
NGC 4478	0.30	0.60	25.8	−2.7	9.8×10^{-3}	1.7×10^{-2}
NGC 4486B	4.68	1.39	−2.2	−39.6
NGC 4494	0.41	0.81	16.9	−12.7	1.5×10^{-2}	1.2×10^{-2}
NGC 4552	0.67	0.72	−51.2	4.8	4.7×10^{-3}	1.9×10^{-3}
NGC 4589	2.08	1.10	−9.4	−8.4	1.6×10^{-2}	3.8×10^{-3}
NGC 4621	0.32	0.98	−11.0	0.1	7.3×10^{-3}	7.6×10^{-4}
NGC 4649	2.44	0.49	−13.8	11.7	9.1×10^{-4}	1.5×10^{-3}
NGC 4660	4.68	1.50	−0.5	−19.0
NGC 4709	0.36	0.38	−21.3	3.0	4.2×10^{-3}	2.7×10^{-3}
NGC 5061	3.24	1.41	−6.2	−115.9	6.8×10^{-3}	2.5×10^{-2}
NGC 5419	0.92	0.27	34.4	−5.7	1.7×10^{-2}	4.7×10^{-3}
NGC 5557	0.48	0.68	45.8	−5.7	3.8×10^{-3}	5.6×10^{-3}
NGC 5576	0.32	0.68	15.5	−2.8	3.9×10^{-3}	4.1×10^{-3}
NGC 5813	0.57	0.51	−64.0	25.4	3.4×10^{-3}	4.7×10^{-3}
NGC 5982	0.27	0.41	−134.6	14.5	4.3×10^{-3}	4.3×10^{-3}
NGC 6849	0.41	0.67	81.8	1.1	5.7×10^{-3}	3.5×10^{-3}
NGC 7213	0.54	0.45	50.2	−18.5	3.3×10^{-2}	6.9×10^{-2}
NGC 7457	0.27	0.53	54.8	−1.7
NGC 7619	0.67	0.71	−3.3	0.4	1.9×10^{-3}	1.9×10^{-3}
NGC 7727	4.68	1.14	15.9	−55.0
NGC 7785	1.99	0.88	3.4	−1.6	8.7×10^{-3}	5.3×10^{-3}
IC 1459	0.50	0.45	41.4	0.1	1.7×10^{-2}	2.2×10^{-3}
IC 4329	0.57	0.37	−62.2	3.0	3.3×10^{-3}	2.1×10^{-3}
ESO 0462-015	0.36	0.83	−97.7	2.0	2.7×10^{-2}	3.1×10^{-3}

Note. — The twist values are measured over the domains of the inner and outer gradients, using the expression in equation (4). γ' gives the local power-law slope of the brightness profile at the twist radius. The outer domain was too limited for twists to be measured for NGC 2778, 3384, 4660, 7457, and 7727. Parameters were also not measured for NGC 4073, 4406, 4486B, and 6876, which have central surface brightness minima.

Table 9. Frequencies of Dust Morphologies

	This paper	Tran et al. (2001)	Lauer et al. (1995)	Total (%)
No dust	39	34	21	94 (53%)
Nuclear rings	14	16	1	31 (18%)
Non-rings	24	23	5	52 (29%)
Total	77	73	27	177 (100%)

Note. — The frequency of dust morphologies in the three papers defining the dust sample is given. “Non-rings” include chaotics (c), spirals (s), and transitional types (t). The second column counts dust morphologies for the present sample. The Tran et al. (2001) column only counts galaxies in that paper not already counted by the present paper; the Lauer et al. (1995) refers to additional galaxies not in the present paper or in Tran et al. (2001).

Table 10. Dust Strength versus Optical Emission Strength: Present Paper

Emission strength	0	1	2	3
Dust Strength > 2.5	0	4	11	2
Dust Strength = 0.3 – 2.5	2	5.5	2.5	0
Dust strength < 0.3	31	7	0	0

Note. — Dust strength vs. optical emission-strength class from Table 3. Galaxies that are too dusty for a reference model (Figure 2) have been assigned dust strengths > 2.5 except for NGC 4786, 5845, 6776, and 7626, which were assigned to the middle dust strength category. Galaxies on bin borders have been assigned to both neighboring bins with half weight. Galaxies with colons on their emission strengths in Table 3 have not been used.

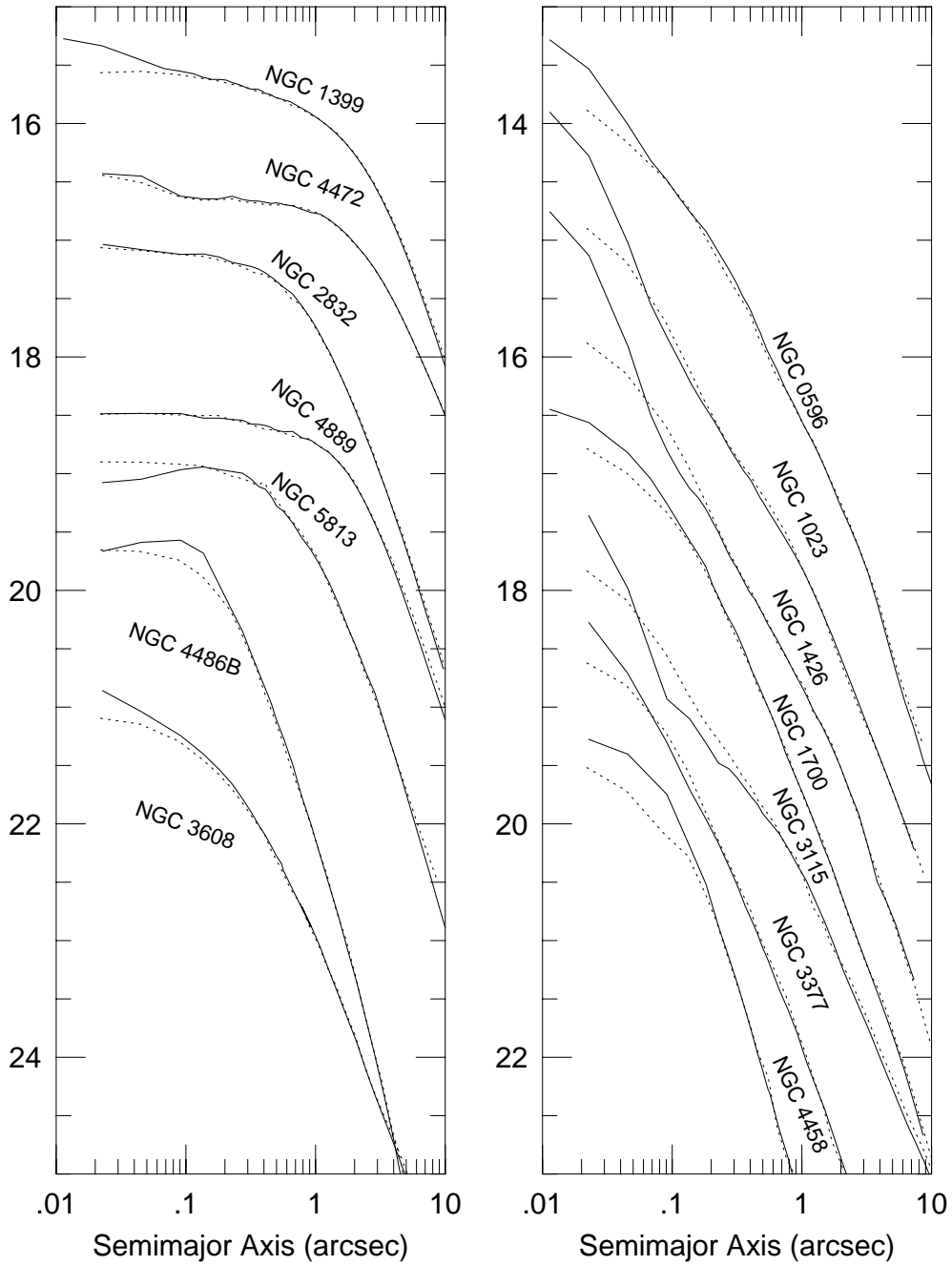


Fig. 4.— Deconvolved WFPC2 brightness profiles (solid lines) are compared to deconvolved WFPC1 profiles (dashed lines) for the same galaxies. The vertical scale is in magnitudes per square arcsecond. The WFPC2 profiles for NGC 2832 and NGC 4889 were published in Laine et al. (2002). All other WFPC2 profiles can also be seen in Figure 3. The WFPC1 and WFPC2 profiles agree extremely well for $r > 0''.1$, except for some galaxies with strong nuclei.

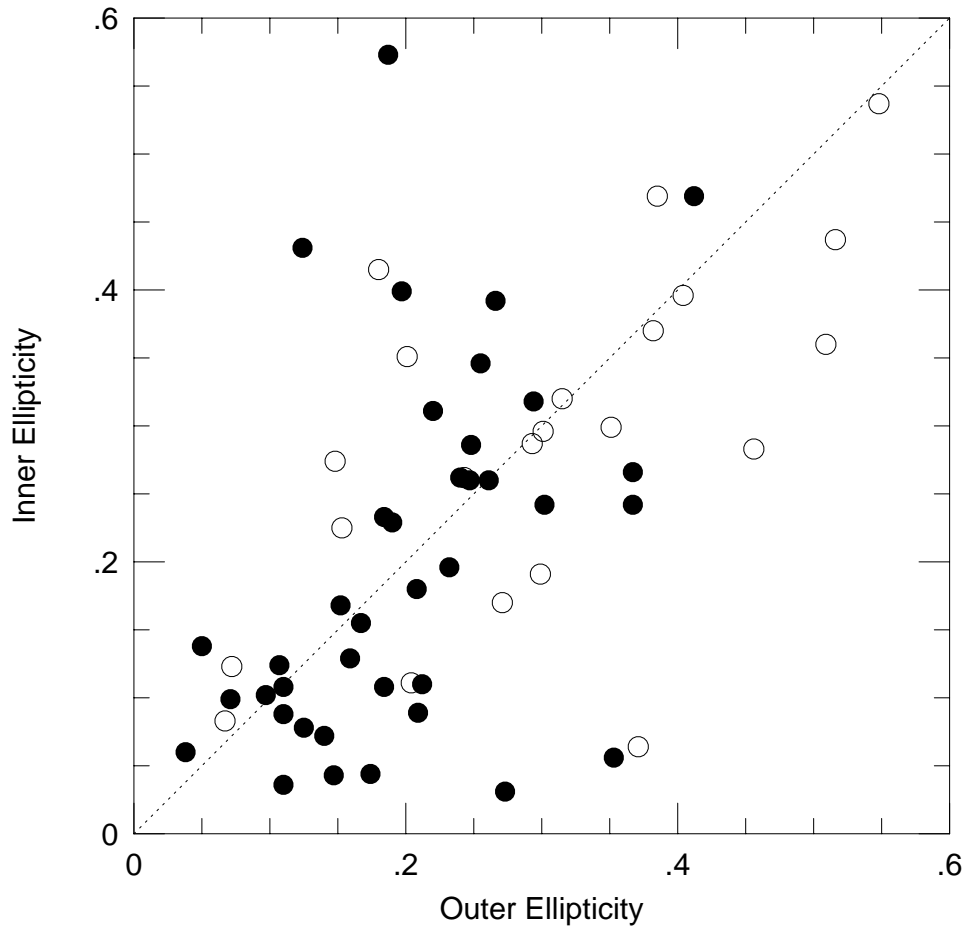


Fig. 5.— Inner ($r \leq r_b$) luminosity-weighted isophote ellipticity is plotted against outer isophote ellipticity. Solid symbols are core galaxies; open symbols are power-law or intermediate galaxies. There is no strong average trend for isophote ellipticity to change with radius for either type of galaxy.

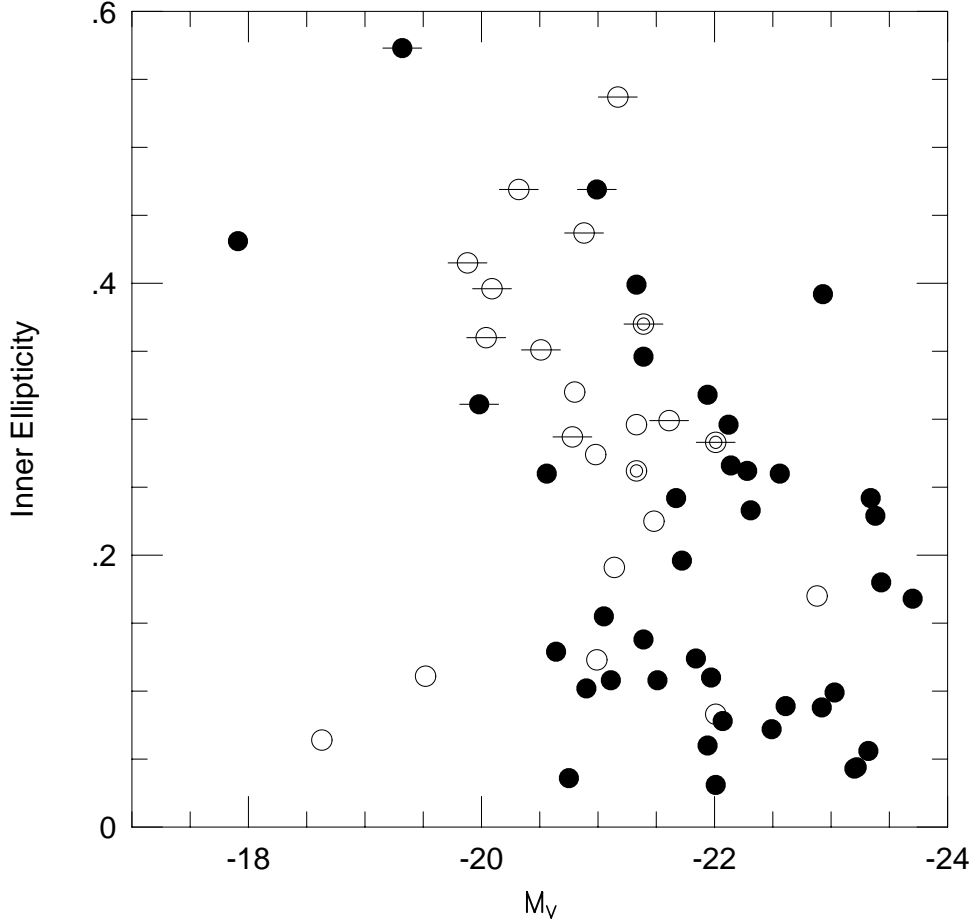


Fig. 6.— Inner ($r \leq r_b$) luminosity-weighted isophote ellipticity is plotted as a function of total galaxy luminosity. Solid symbols are core galaxies, open symbols are power-law galaxies, and intermediate galaxies are plotted as double open circles. Galaxies with *inner* stellar disks are indicated with horizontal lines. Power-law galaxies tend to have higher inner ellipticity than core galaxies. Nearly all power-law galaxies with $\epsilon \geq 0.3$ have inner disks, implying that they are also present in the rounder power-law galaxies, but are not seen due to unfavorable viewing angles. Disks are visible in flattened core and intermediate galaxies fainter than $M_V \approx -21$, suggesting that these are transitional objects. Disks are not seen in bright core galaxies.

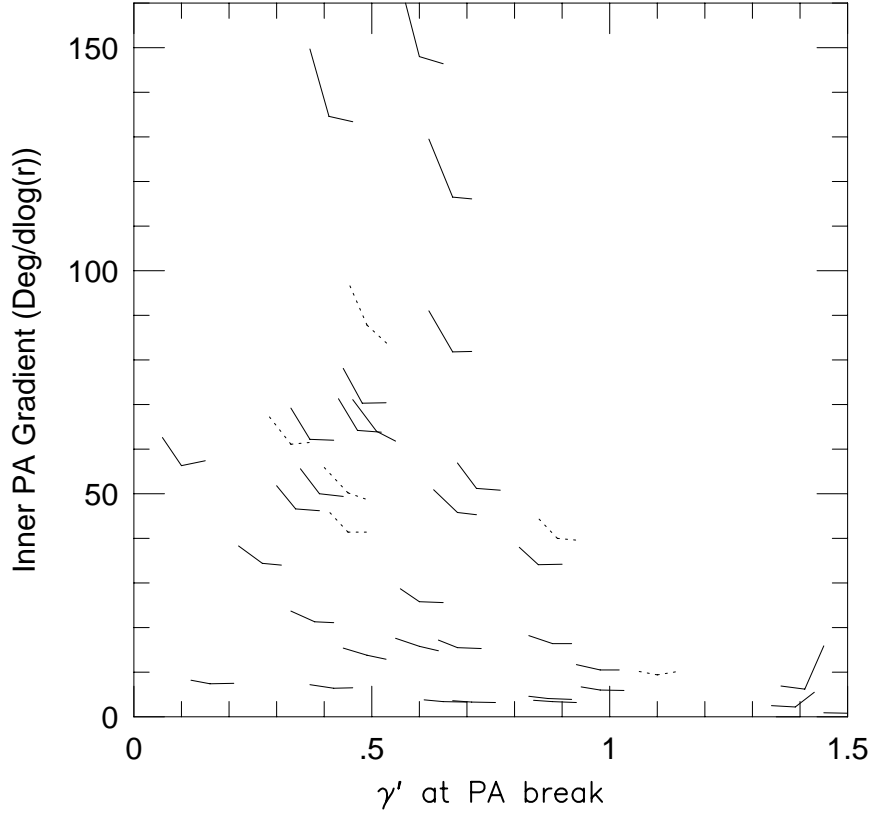


Fig. 7.— Absolute value of the inner gradients in isophote position angle for core galaxies only are plotted as a function of the local logarithmic surface brightness slope, γ' , at the radius dividing the inner and outer gradients. The wedge symbols also encode the value of the inner gradients in the slope of their left line segments and the outer gradients in the right segments. Dotted symbols are those galaxies that may be strongly affected by dust. Radii of the break or “hinge” in the PA gradients cluster near $\gamma' = 0.5$, which lies well within the break radii.

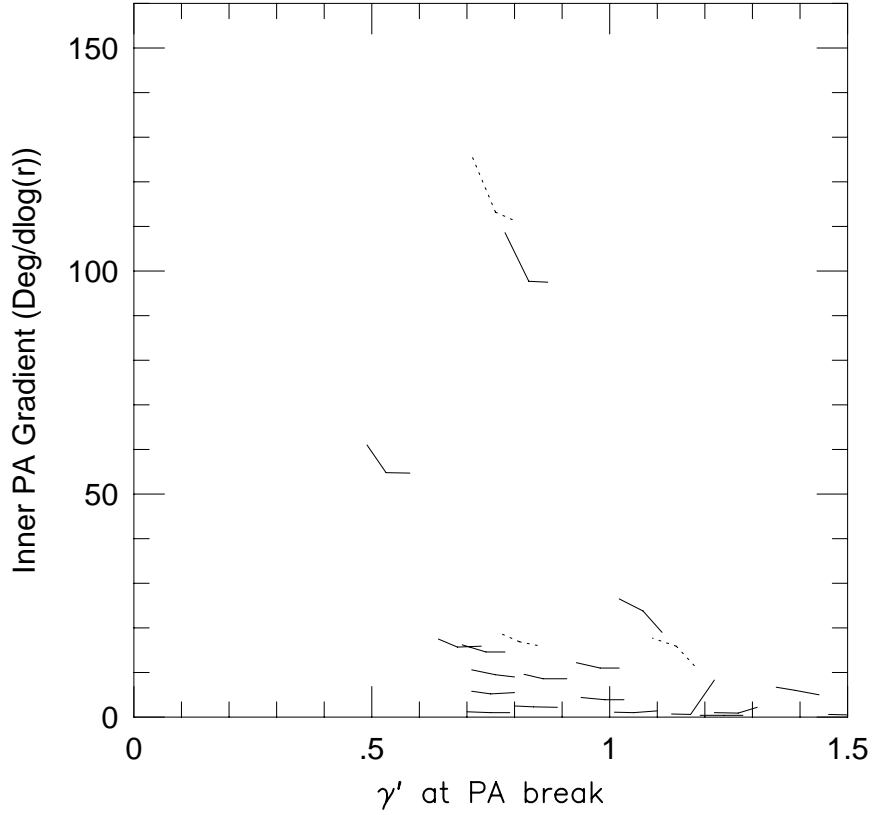


Fig. 8.— Absolute value of the inner gradients in isophote position angle for the intermediate and power-law galaxies are plotted as a function of the local logarithmic surface brightness slope, γ' , at the radius dividing the inner and outer gradients. The wedge symbols also encode the value of the inner gradients in the slope of their left line segments and the outer gradients in the right segments. Dotted symbols are those galaxies that may be strongly affected by dust. Radii of the break or “hinge” in the PA gradients cluster near $\gamma' = 1$, larger than for core galaxies (Figure 7). PA twists are also smaller than for core galaxies, but the text shows that the relative amounts of light involved in the twist phenomenon is the same in both types of galaxy.

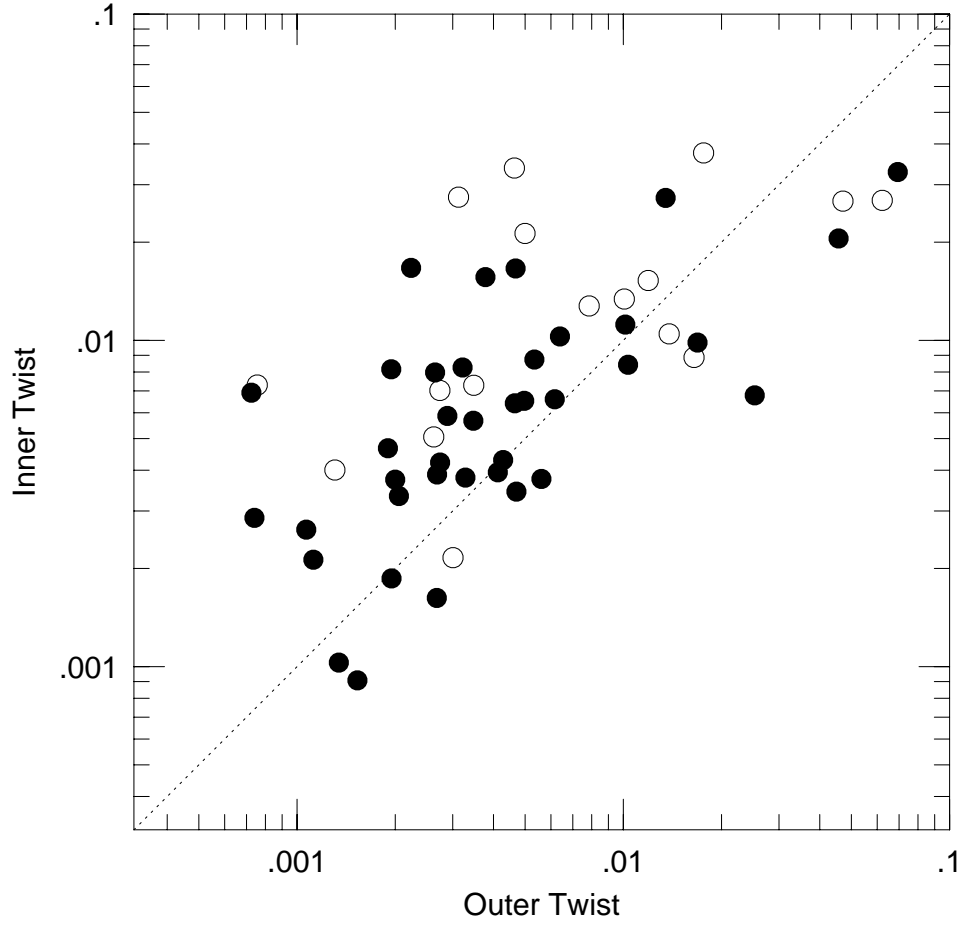


Fig. 9.— Position angle twists defined using equation (4) for inner radii are plotted versus the twists for the outer radii. Solid symbols are core galaxies; open symbols are power-law or intermediate galaxies. Twists are larger in inner regions, but the intrinsic strength of twists in core and power-law galaxies is similar.

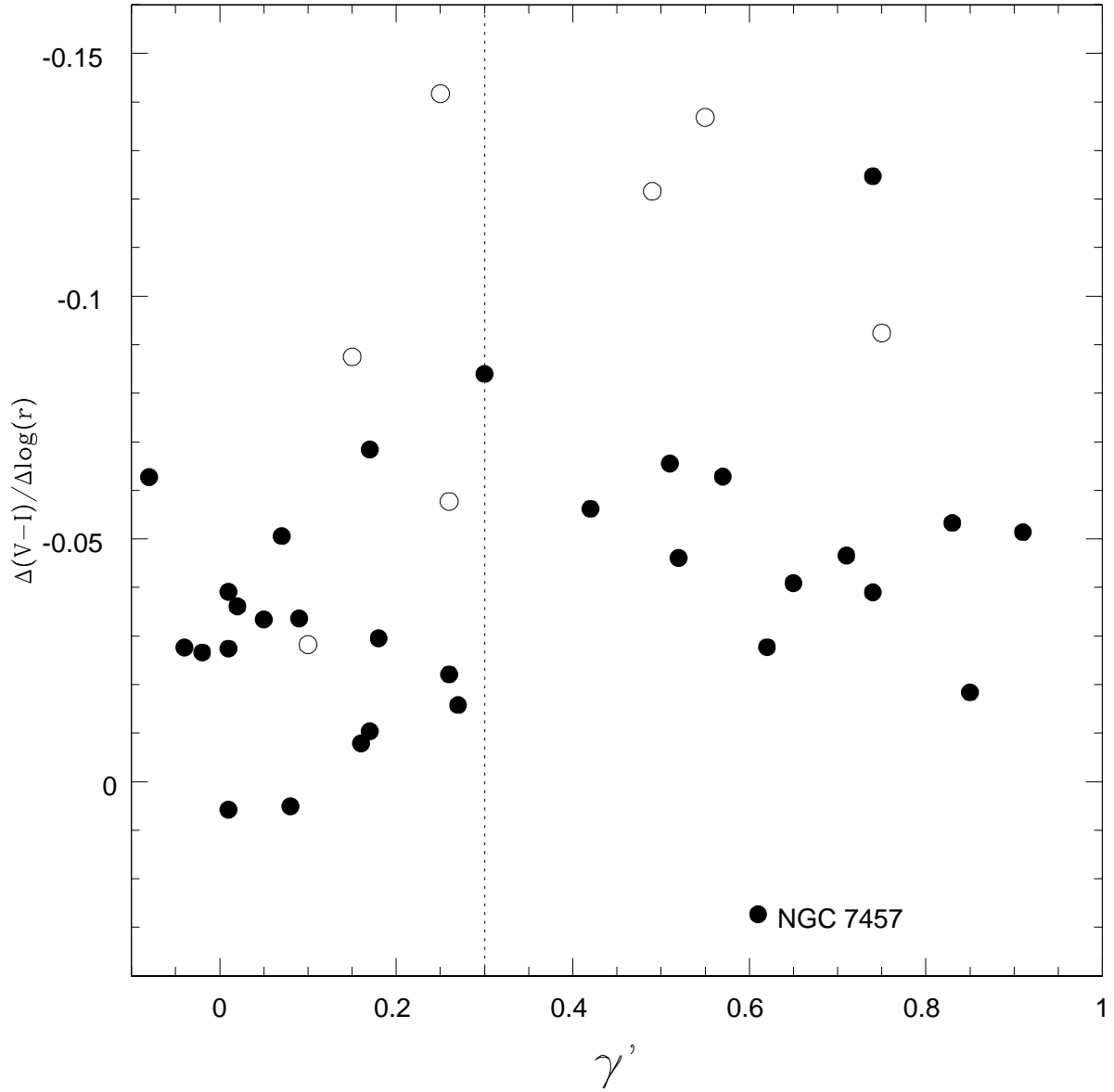


Fig. 10.— Slopes of the inner $V - I$ color gradients as a function of γ' ; the vertical line separates core from power-law and intermediate galaxies. Open symbols are those galaxies that may be strongly affected by dust. After eliminating dusty galaxies, power-law galaxies are seen to have gradients only slightly steeper than core galaxies.

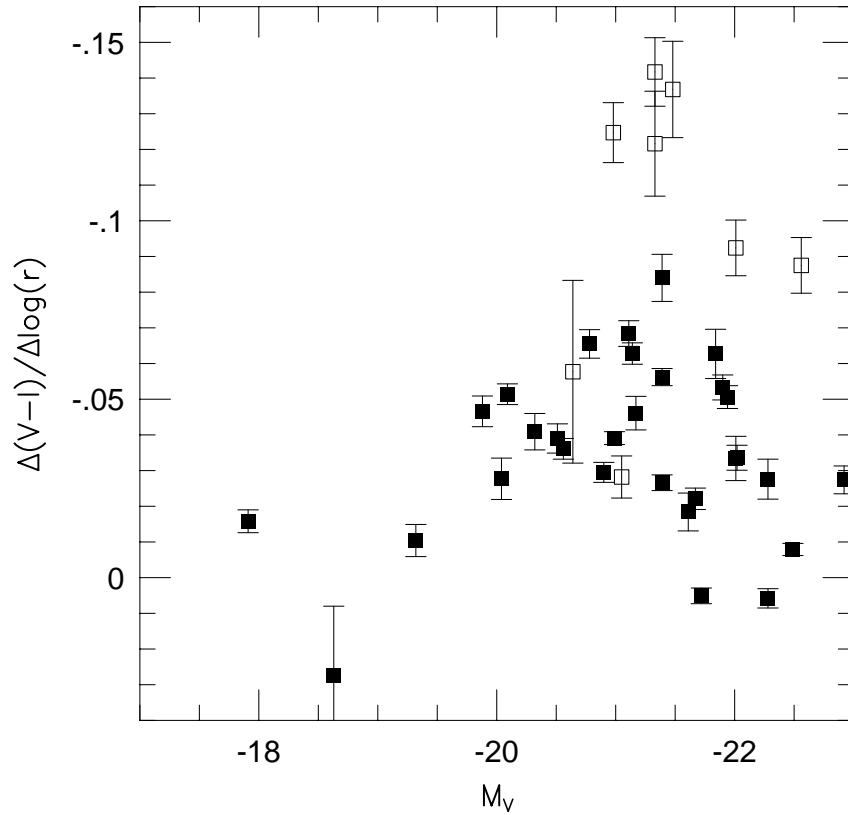


Fig. 11.— Slopes of the inner $V - I$ color gradients as a function galaxy luminosity. Open symbols are those galaxies that may be strongly affected by dust. After these are eliminated, there is little remaining trend in color gradient versus absolute magnitude.

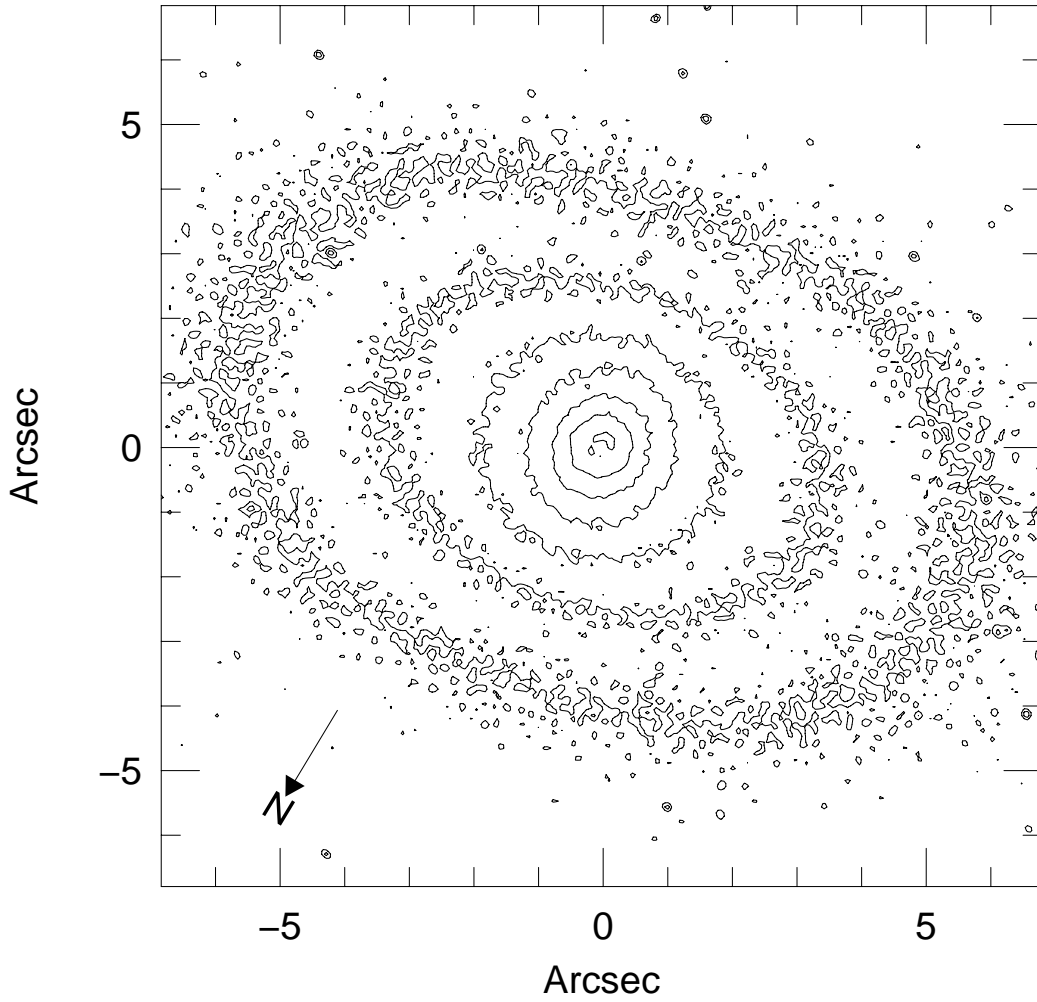


Fig. 12.— Contour plot (V band) of the center of the central-minimum galaxy NGC 4073. The contours are spaced in 0.5 mag increments; the innermost contour is at $\mu_V = 16.43$ and has been selected to highlight asymmetries in the ring of light surrounding the central minimum.

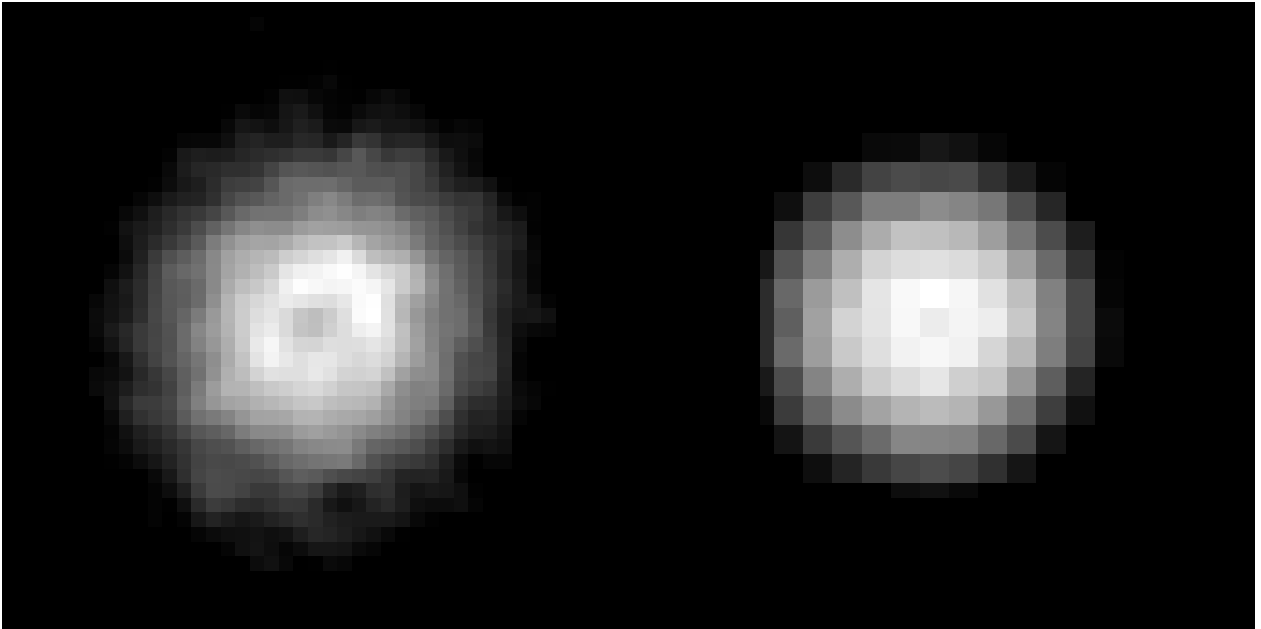


Fig. 13.— Central images of the central-minimum galaxy NGC 4073. The image on the left is the central $2'' \times 2''$ region of the deconvolved WFPC2 F555W image. A hard contrast stretch has been used to bring out the central minimum. The image on the right is the NICMOS-2 H band image (from program GTO 7820) as observed. The NICMOS-2 pixels have been doubled in size to approximate the WFPC2 scale. The orientation of both images is arbitrary. The presence of the minimum in H band suggests that it is not due to dust.

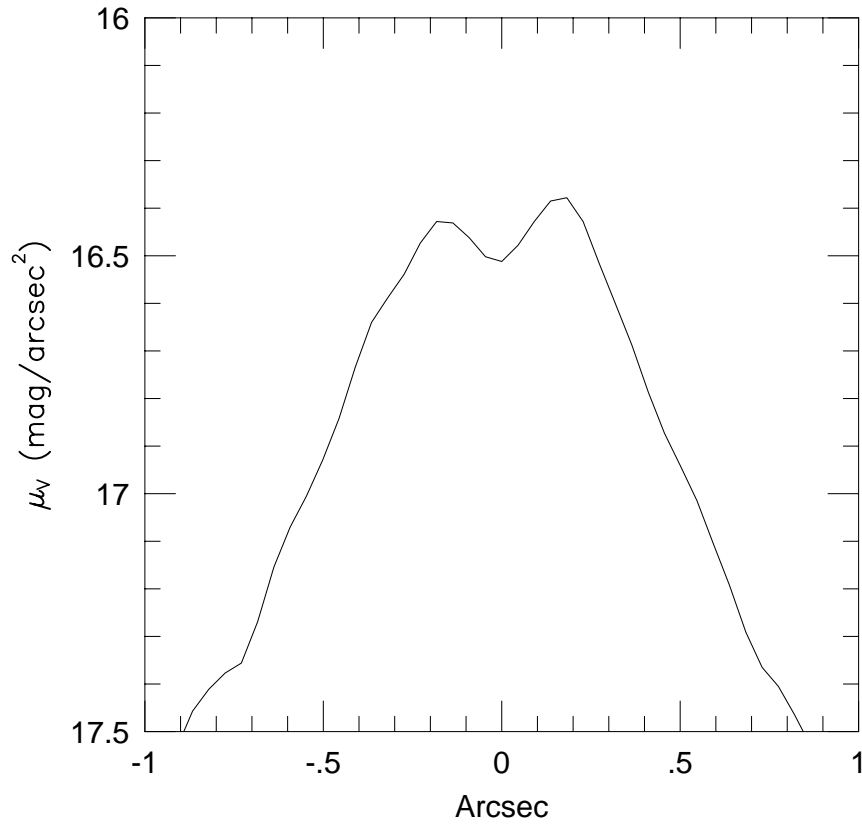


Fig. 14.— This figure shows a 3-pixel wide cut taken through the center of the central-minimum galaxy NGC 4073 (*V* band) at position angle 166°.

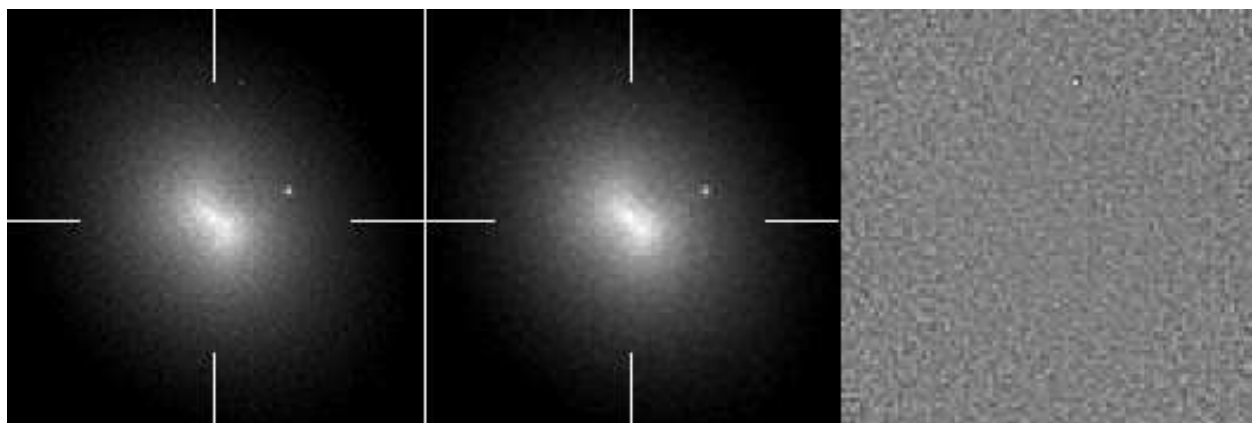


Fig. 15.— The central $4'' \times 4''$ portions of the deconvolved V and I band images of the central-minimum galaxy NGC 4382 are shown. Tickmarks indicate the galaxy center. The panel on the right is a ratio of the V to I image, showing that there is no central dust absorption. See Figure 16 for orientation.

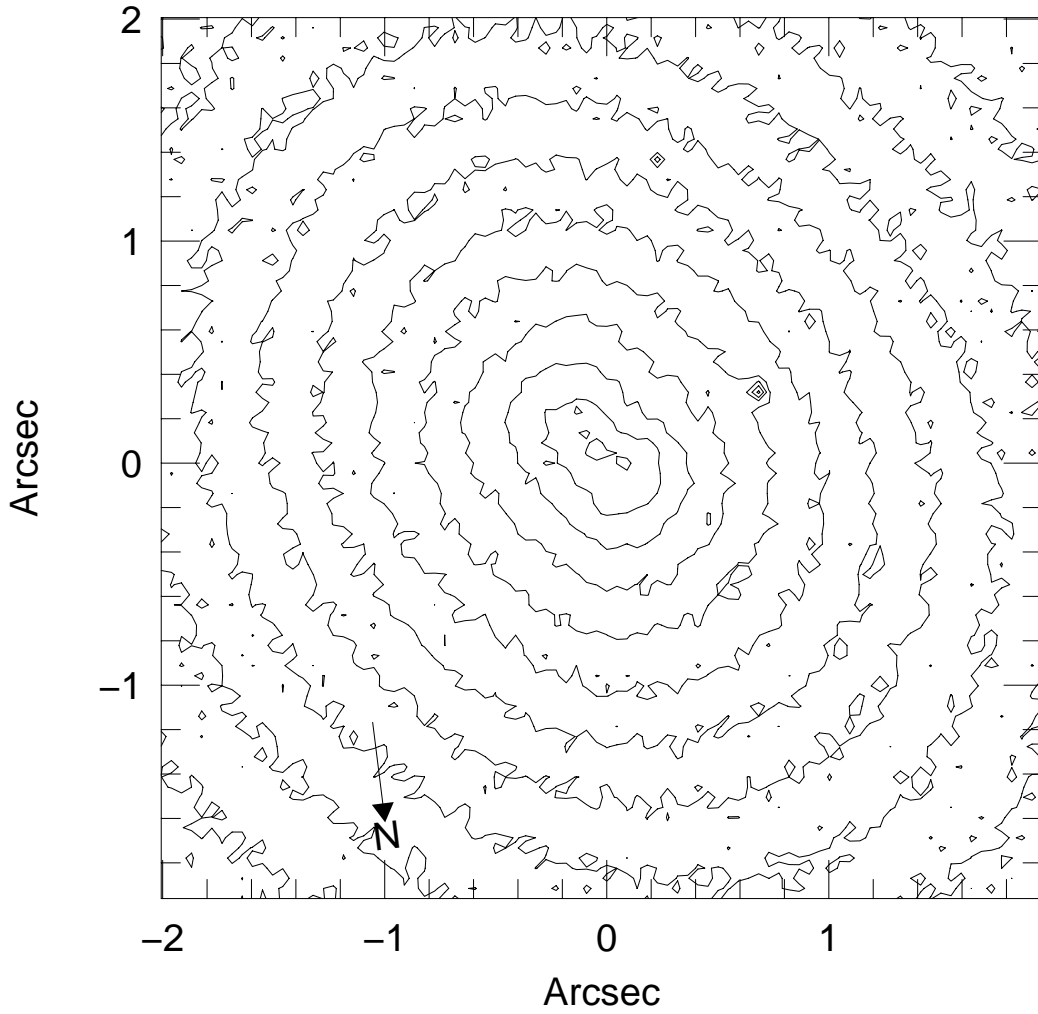


Fig. 16.— Contour plot of the center of the deconvolved V band image of the central-minimum galaxy NGC 4382. Contours are in steps of 0.2 mag in surface brightness. The innermost contour is at $\mu_V = 14.84$ and is selected to highlight the peaks of the double nucleus.

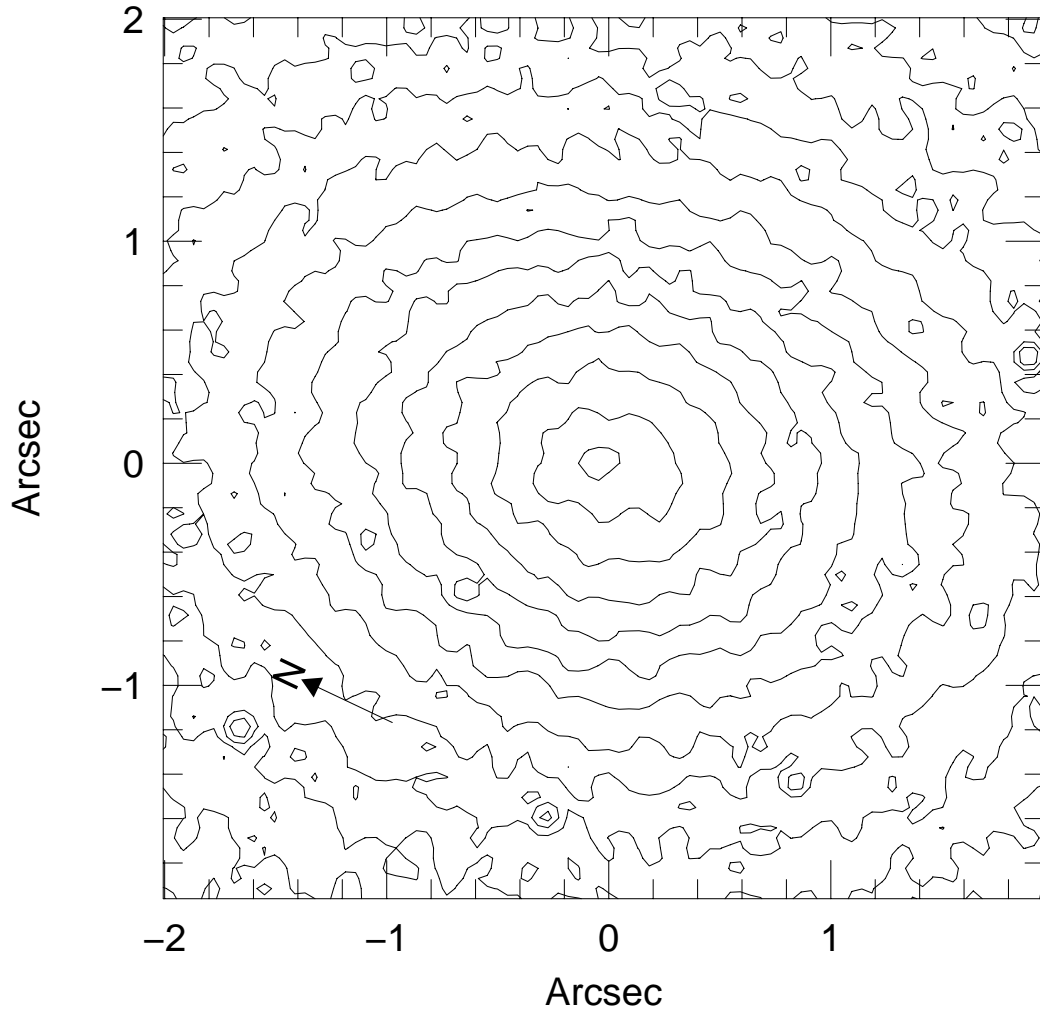


Fig. 17.— Contour plot of the center of the deconvolved V band image of the offset-center galaxy NGC 507. Contours are in steps of 0.2 mag in surface brightness. The innermost contour is at $\mu_V = 16.24$ and is selected to highlight the central asymmetry of the brightness distribution. It may be that NGC 507 is like M31 or NGC 4382 seen at lower resolution.

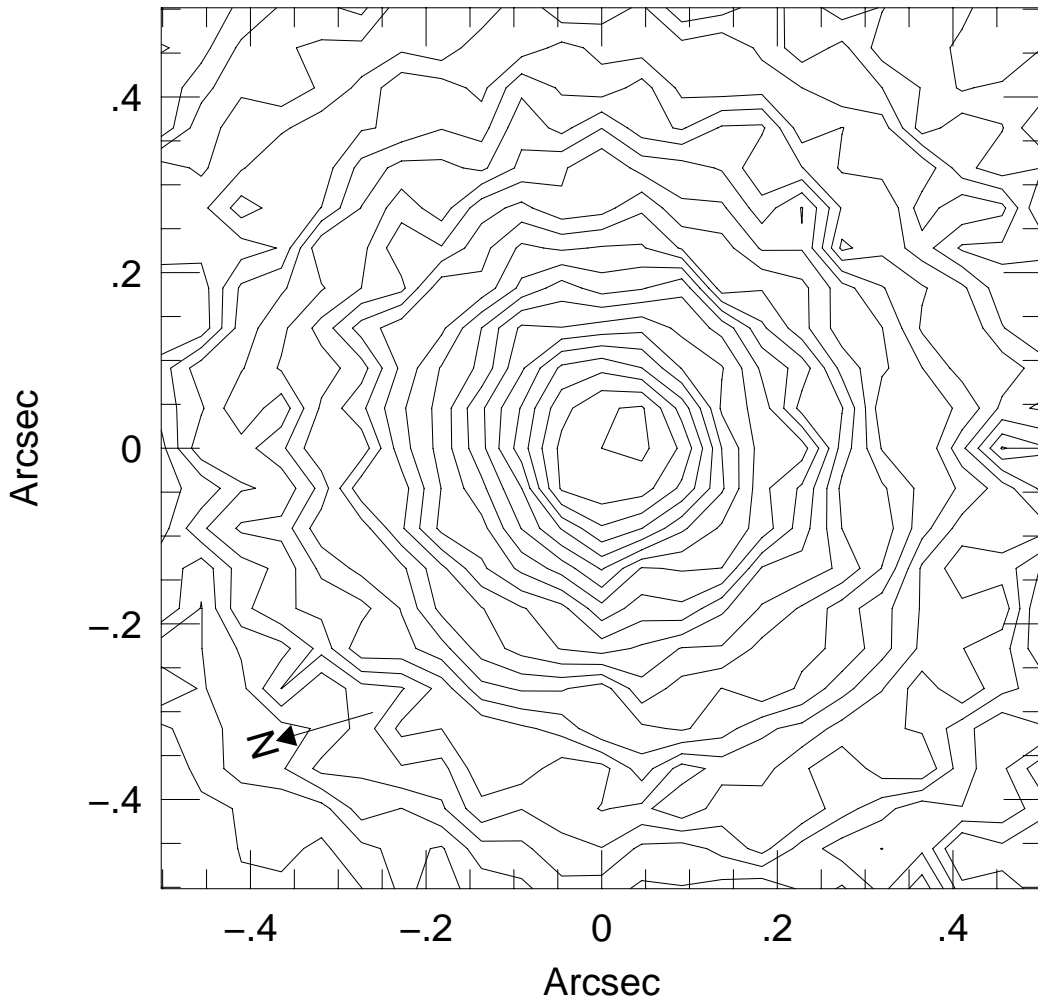


Fig. 18.— Contour plot of the center of the deconvolved V band image of the offset-center galaxy NGC 1374. Contours are in steps of 0.1 mag in surface brightness. The innermost contour is at $\mu_R = 13.73$ and is selected to highlight the central asymmetry of the brightness distribution. It may be that NGC 1374 is like M31 or NGC 4382 seen at lower resolution.

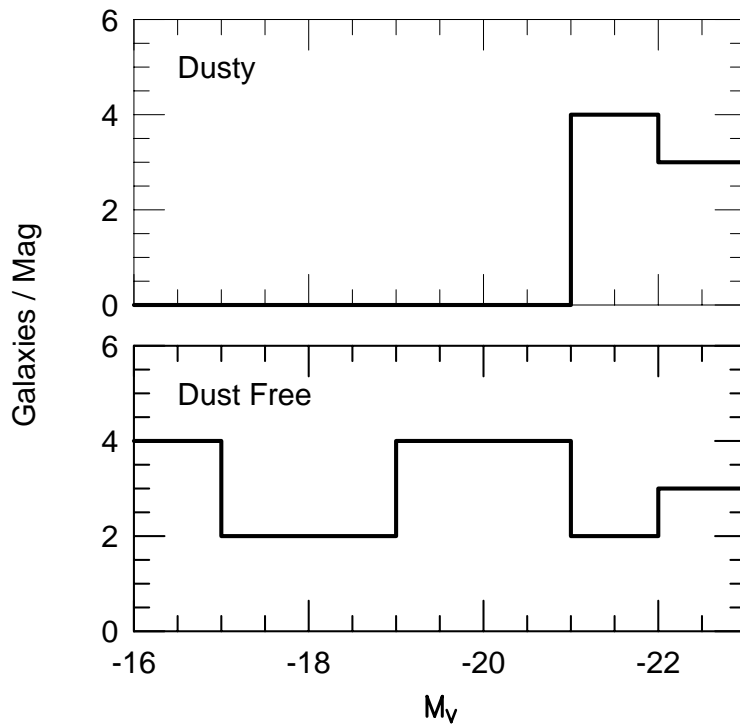


Fig. 19.— Occurrence of dust clouds in Virgo cluster elliptical galaxies is shown as a function of luminosity. Histogram bins are one magnitude wide. All galaxies fainter than $M_V = -21$ in Virgo are dust free.

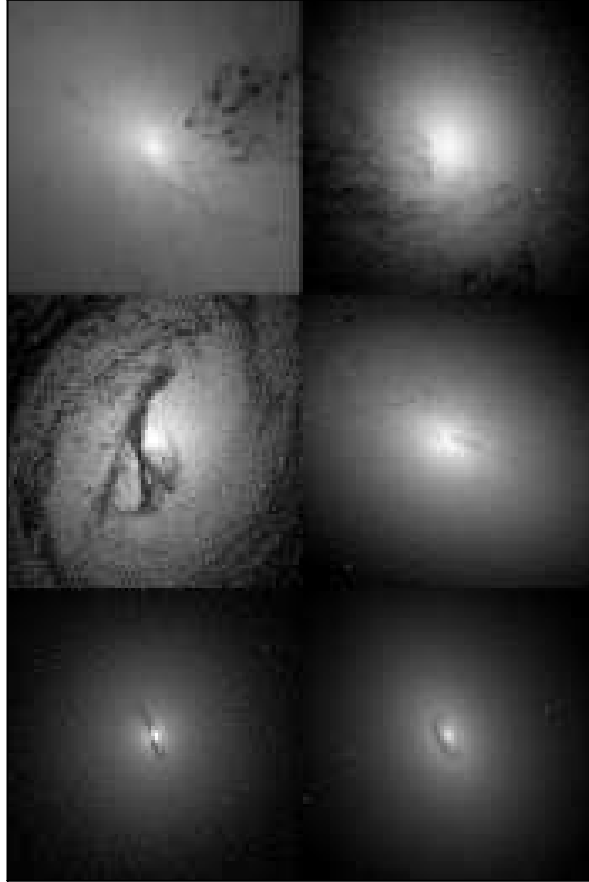


Fig. 20.— Six galaxies have been selected to illustrate a hypothetical dust-settling sequence. NGC 1316 is the galaxy in the top left panel and has the most poorly organized dust. Top right is NGC 4278, in which the dust appears to be streaming towards the nucleus. Center panels are NGC 3607 (left) and IC 1459, in which a central dust ring is starting to be organized. Bottom left is NGC 2434, which has a slightly warped ring. NGC 4494, having a symmetric ring, is the final galaxy in the sequence. Each panel is $8''$ on a side; deconvolved images have been used.

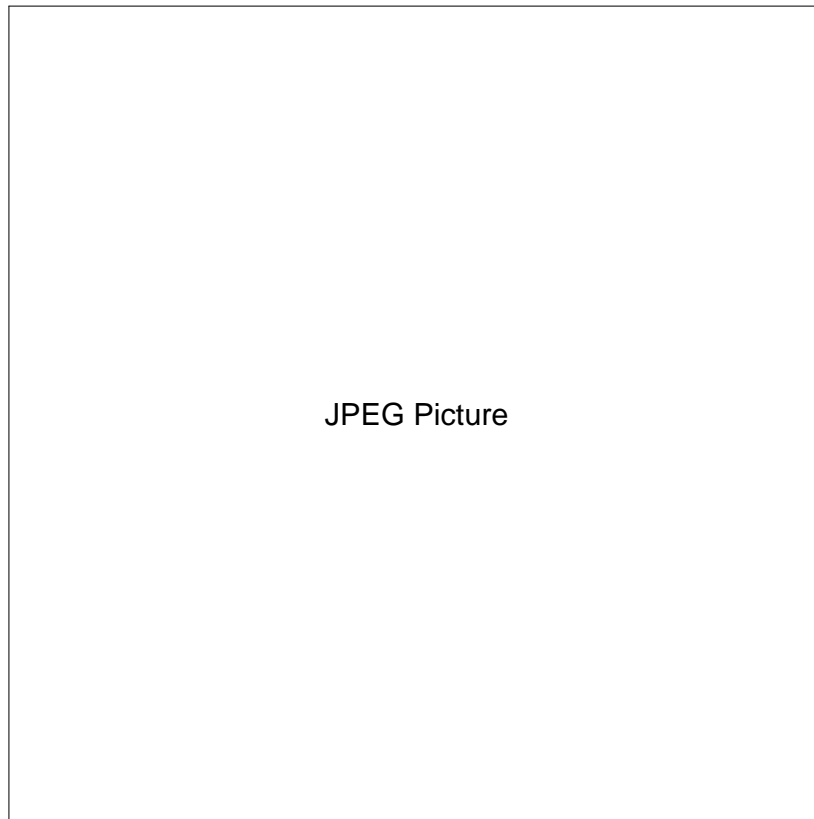


Fig. 21.— The deconvolved V-band image of NGC 3607. A logarithmic intensity stretch has been used. The image is 512 pixels or $23''.3$ on a side. The outer dust pattern is remarkably symmetric and tightly wrapped, signifying a dust disk with a well-defined plane and great age. By contrast, the inner dust seems to be settling to a plane that is *highly inclined* to the outer plane and gives the appearance of being dynamically much younger. Nevertheless, the two structures appear to join smoothly.

This figure "lauer_fig_01_1.jpg" is available in "jpg" format from:

<http://arxiv.org/ps/astro-ph/0412040v1>

This figure "lauer_fig_03_01.gif" is available in "gif" format from:

<http://arxiv.org/ps/astro-ph/0412040v1>

This figure "lauer_fig_01_2.jpg" is available in "jpg" format from:

<http://arxiv.org/ps/astro-ph/0412040v1>

This figure "lauer_fig_02.jpg" is available in "jpg" format from:

<http://arxiv.org/ps/astro-ph/0412040v1>

This figure "lauer_fig_03_02.gif" is available in "gif" format from:

<http://arxiv.org/ps/astro-ph/0412040v1>

This figure "lauer_fig_01_3.jpg" is available in "jpg" format from:

<http://arxiv.org/ps/astro-ph/0412040v1>

This figure "lauer_fig_03_03.gif" is available in "gif" format from:

<http://arxiv.org/ps/astro-ph/0412040v1>

This figure "lauer_fig_01_4.jpg" is available in "jpg" format from:

<http://arxiv.org/ps/astro-ph/0412040v1>

This figure "lauer_fig_03_04.gif" is available in "gif" format from:

<http://arxiv.org/ps/astro-ph/0412040v1>

This figure "lauer_fig_03_05.gif" is available in "gif" format from:

<http://arxiv.org/ps/astro-ph/0412040v1>

This figure "lauer_fig_03_06.gif" is available in "gif" format from:

<http://arxiv.org/ps/astro-ph/0412040v1>

This figure "lauer_fig_03_07.gif" is available in "gif" format from:

<http://arxiv.org/ps/astro-ph/0412040v1>

This figure "lauer_fig_03_08.gif" is available in "gif" format from:

<http://arxiv.org/ps/astro-ph/0412040v1>

This figure "lauer_fig_03_09.gif" is available in "gif" format from:

<http://arxiv.org/ps/astro-ph/0412040v1>

This figure "lauer_fig_03_10.gif" is available in "gif" format from:

<http://arxiv.org/ps/astro-ph/0412040v1>

This figure "lauer_fig_03_11.gif" is available in "gif" format from:

<http://arxiv.org/ps/astro-ph/0412040v1>

This figure "lauer_fig_03_12.gif" is available in "gif" format from:

<http://arxiv.org/ps/astro-ph/0412040v1>

This figure "lauer_fig_03_13.gif" is available in "gif" format from:

<http://arxiv.org/ps/astro-ph/0412040v1>

This figure "lauer_fig_03_14.gif" is available in "gif" format from:

<http://arxiv.org/ps/astro-ph/0412040v1>

This figure "lauer_fig_03_15.gif" is available in "gif" format from:

<http://arxiv.org/ps/astro-ph/0412040v1>

This figure "lauer_fig_03_16.gif" is available in "gif" format from:

<http://arxiv.org/ps/astro-ph/0412040v1>

This figure "lauer_fig_03_17.gif" is available in "gif" format from:

<http://arxiv.org/ps/astro-ph/0412040v1>

This figure "lauer_fig_21.jpg" is available in "jpg" format from:

<http://arxiv.org/ps/astro-ph/0412040v1>